Dear Reviewers，

We are truly grateful for the critical comments and thoughtful suggestions provided by you. Based on these comments and suggestions, we have made careful modifications to the original manuscript. All changes made to the text are marked in red font. The main corrections in the paper and the responses to your comments are listed below. We are at your disposal for any further information and willing to improve further our manuscript by adding the considerations provided in our reply. Kind regards.

(1) The elastic model does not overlap fully in time with the GPS time series, will it influence the results?

Response: The elastic correction needs a high-resolution model of surface mass variation, and then the mass changes are converted into displacements using Green's functions. However, because of the lack of observed data and the data fusion problem, accurately quantifying elastic corrections are difficult. In this paper, we assume that the elastic velocity remains constant for nearly 20 years. The elastic model of Riva et al. (2017) is used to compute the elastic velocity to explore the noise and CME effects on GIA assessments. Then, the effects on GPS velocity estimates are revealed, with the results providing a reference for future research.

(2) The introduction needs more complete review of the assessment GIA models.

Response: We have added the relevant content:

"Martín-Español et al. (2016) used the elastic-corrected GPS vertical velocities in Antarctica over the period 2009-2014 to asses 8 GIA models, including forward and inverse methods, and they found systematic underestimations of the GPS rates over specific regions characterized by low mantle viscosities and thin lithosphere. Liu et al. (2018) applied ICA and PCA for 53 GPS stations from 2010 to 2014 and used the white noise plus power law (PL) noise model to estimate GPS velocities, and after correction for elastic effects, they assessed the consistency among 4 GIA models and GPS vertical velocities. They that the consistency between the GPS observed velocities and GIA models were generally improved after spatiotemporal filtering. Martín-Español et al. (2016) and Liu et al. (2018) used 53 GPS stations' velocities to assess the GIA models, although Martín-Español et al. (2016) did not perform filtering, and both studies considered only one noise model. A uniform criterion is not available to judge the effects of CME and noise models; therefore, a quantify study is needed of the effects based on GPS velocity estimates and GIA assessments. In this paper, we used more than 79 stations with long time series (around 9 years) to achieve an accurate velocity, and then the influence of common mode error (CME) and 5 noise models on the GPS accuracy was analyzed. Finally, we assessed the application of GIA models in Antarctica."

(3) Can you more precisely describe the noise models before and after filtering?

Response: To explore the effect of noise, we used a noise-free model and 5 noise models to estimate the GPS velocities before and after filtering: white noise plus power low noise (WN+PN), white noise plus random walk noise (WN+RW), white noise plus flicker noise (WN+FN), white noise plus power low noise plus random walk noise (WN+FN+RW), and white noise plus random walk noise plus generalized Gauss-Markov (WN+RW+GGM).

(4) GNSS and GPS are inconsistency, GNSS in title but GPS throughout all the paper.
Response: We have changed the GNSS to GPS.

(5) P6L7-14: the discussed stations need some introductions to explain further. Are these stations with large differences to previous results?
Response: We have added the following introduction: “The GPS data time span also has an important effect on the velocity estimate, such as CAPF, located in NAP……” These stations present large differences relative to previous results. We think this is due to both the data and filtering (as described in Section 3.1); thus, the GPS data time span has an important effect on the velocity estimates, which are significantly different than previous results (we also compared the velocities between our results and Martín-Español et al., 2016, and the difference varied between 0 and 7 mm/yr), which shows that the time span will directly affect the results of the GIA evaluation. Further study is required to quantify their respective impacts, which is beyond the scope of this study.

(6) P4L17: the definition of ’residual’ is same as the residual series in Section 2.1?

Response: It has some little difference and we have revised the “residual time series” to “the RegEM interpolated coordinate time series (the trend, annual and semiannual terms are removed)”

(7) Figure 2 and Figure 5 are not clear, difficult to see the details. It is better to expand the cales.

Response: We have revised the scale and provided the original vector graphs in the attachments (the name of figure 2 and figure 5 has changed to figure 3 and figure 6)

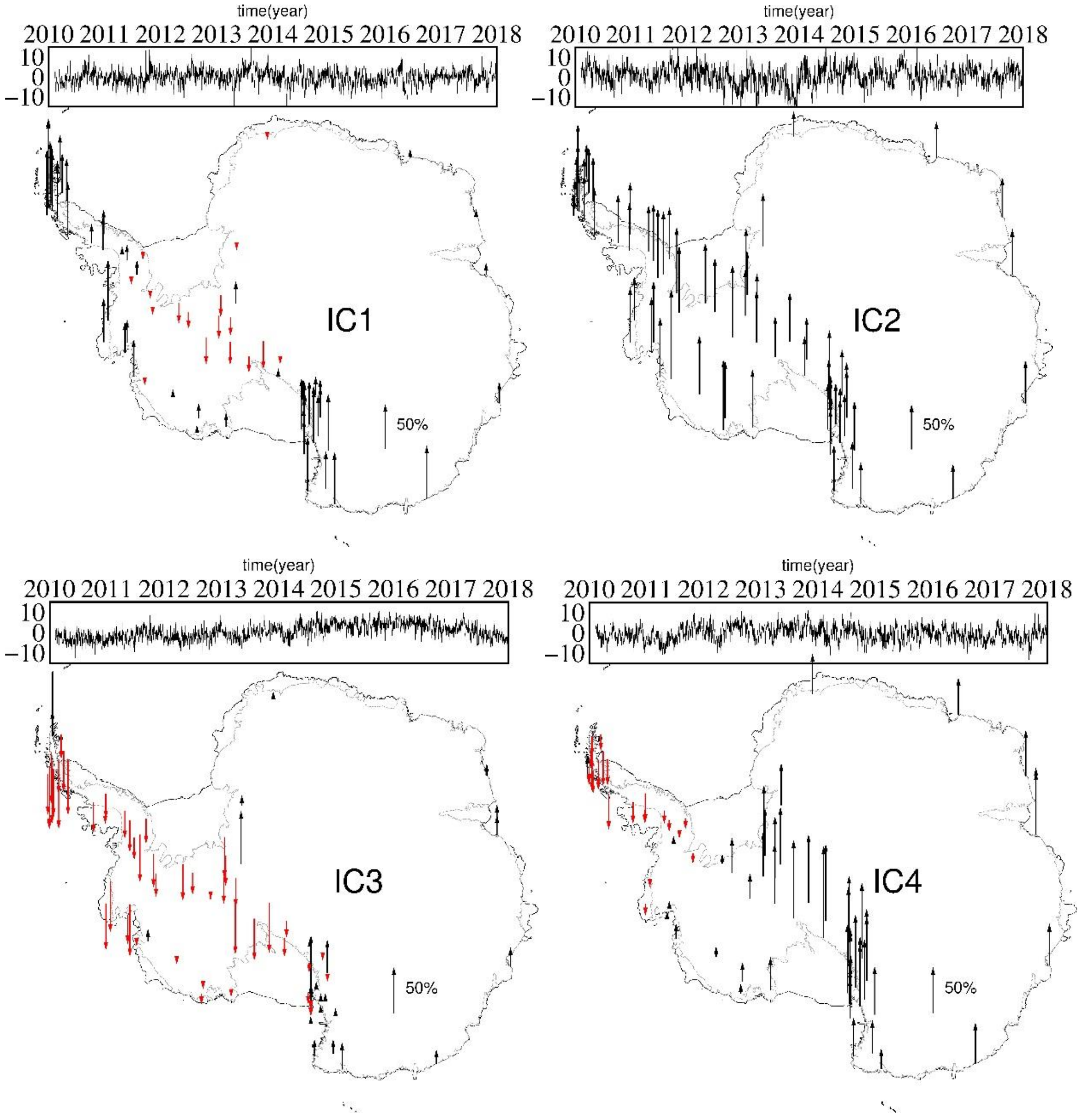
time(year)
2010 2011 2012 2013 2014 2015 2016 2017 2018
10
0
−10
IC1
50%
time(year)
2010 2011 2012 2013 2014 2015 2016 2017 2018
10
0
−10
IC2
50%
time(year)
2010 2011 2012 2013 2014 2015 2016 2017 2018
10
0
−10
IC3
50%
time(year)
2010 2011 2012 2013 2014 2015 2016 2017 2018
10
0
−10
IC4
50%

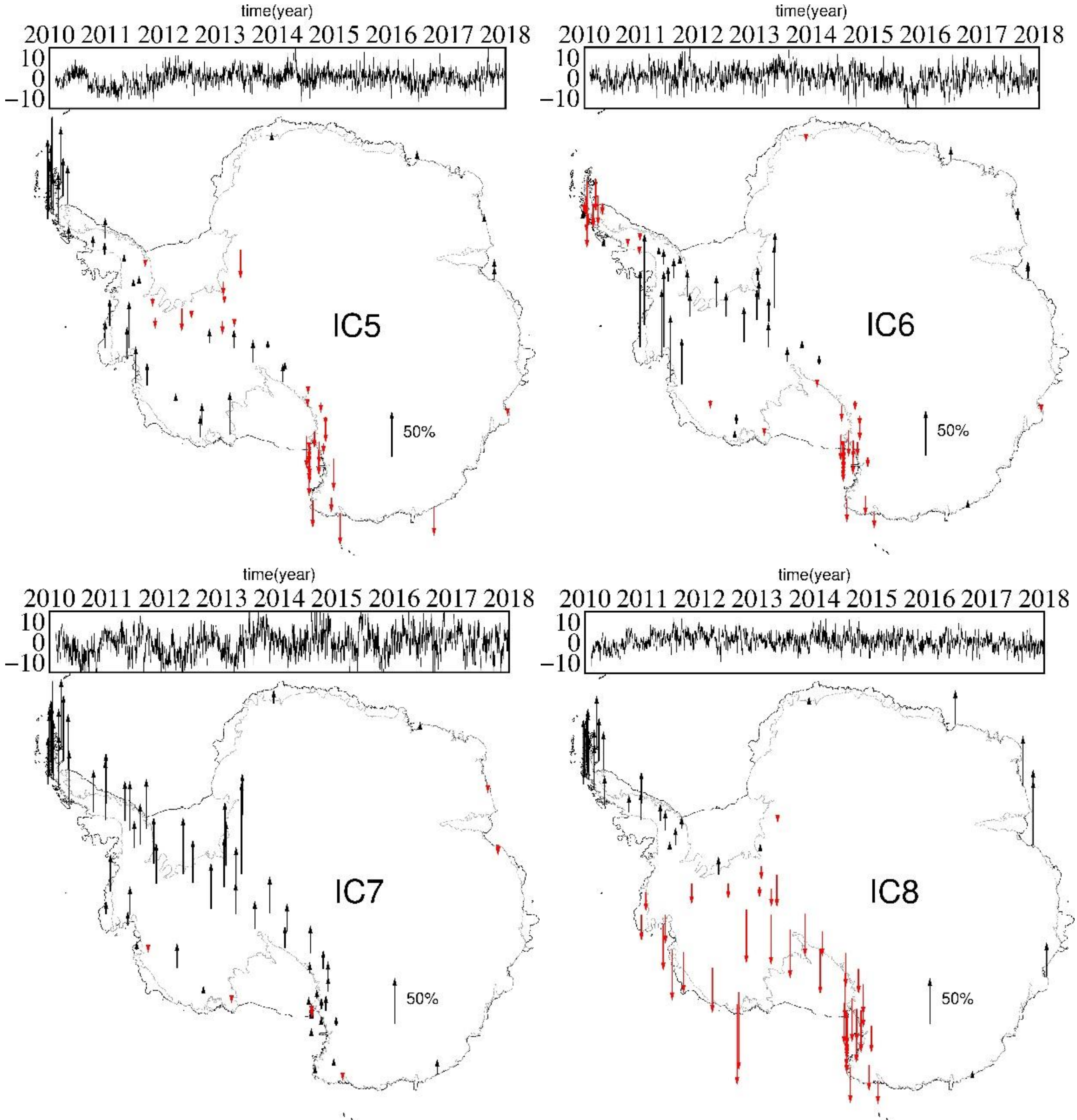

Figure 3. Results of the IC1-IC8 components (the black arrows are a positive spatial response, and the red arrows are a negative spatial response)

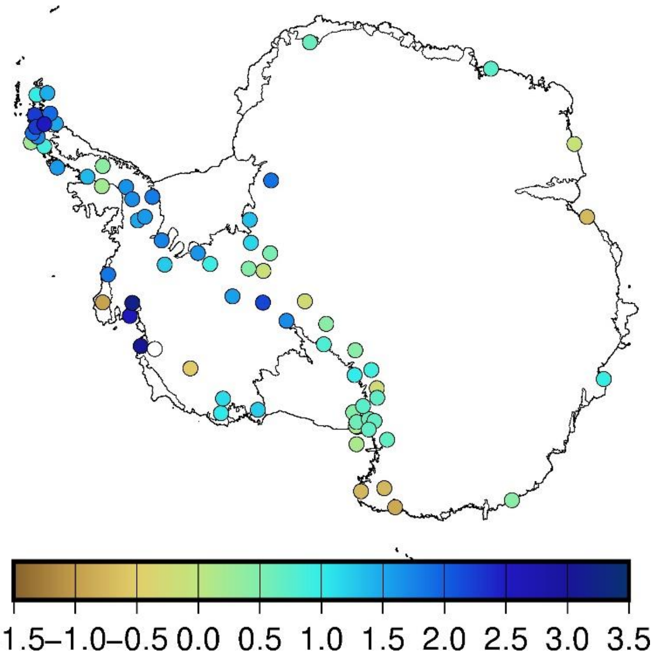

Figure 6. GPS velocity field after applying the noise analysis and AIC filter (mm yr^{-1})

An assessment of GIA solutions based on high-precision GPS velocity field for Antarctica

Wenhao Li[1], Fei Li[1,2], Shengkai Zhang[1], Jintao Lei[3], Qingchuan Zhang [1], Feng Xiao[1], Lexian Yuan[4]

[1]Chinese Antarctic Center of Surveying and Mapping, Wuhan University, Wuhan 430079, China;
[2]State Key Laboratory of Information Engineering in Surveying，Mapping and Remote Sensing，Wuhan University，Wuhan 430079, China;
[3]Department of Land Surveying and Geo-Informatics, Hong Kong Polytechnic University, Hung Hom 999077, Hong Kong, China;
[4]Changjiang Spatial Information Technology Engineering Co., Ltd., Wuhan 430010, China；
Correspondence to: Fei Li（fli@whu.edu.cn)

Abstract. Past changes in mass loading, especially LGM (Last Glacial Maximum), may cause the viscoelastic response of the Earth, this phenomenon is the so-called glacial isostatic adjustment (GIA). GIA includes the horizontal and vertical motions of the crust, the gravity field and rotation axis of the earth. Due to the uncertainties in the ice loading history and the mantle viscosity, modeling GIA will be difficult and challenging in Antarctica. The GPS velocity field provides an effective method to constrain the GIA vertical velocity; however, to obtain the high-precision GPS velocity field, we must consider the effects of common mode error（CME）and the choice of optimal noise model (ONM). We used independent component analysis (ICA) to remove the CME recorded at 79 GPS stations in Antarctica and determined the ONM of GPS time series based on the Akaike information criterion (AIC). Then, the high-precision GPS velocity field is obtained; we used the high-precision GPS velocity field to assess the application of GIA models in Antarctica. The results show that the maximal GPS velocity variation is up to 1.2 mm yr^{-1}, and the mean variation is 0.2 mm yr^{-1}. We find systematic underestimations of all GIA model velocities in the Amundsen Sea area (ASE). Because the upper mantle viscosities in the NAP are lower than those in the south Antarctic Peninsula (SAP), the GPS vertical velocities in NAP regions are larger than SAP regions. In the Filcher-Ronne Ice Shelves(FRIS), the observed GPS velocity and predicted GIA model velocity are consistent. In East Antarctica (EA), the vertical motion is nonsignificant, and the GIA and ice loading have a small impact in this area.

1 Introduction

GIA is the solid Earth's viscoelastic response to past changes in ice-ocean loading. GIA influences crustal displacements, the geoid and regional sea level patterns（Wang et al., 2008；Ivins et al., 2013；Argus et al., 2010; Hao et al., 2016）; we can obtain the GIA vertical velocity through forward models (Peltier, 2004), inverse models (Riva et al. 2009) and geodetic observations (such as GPS; King et al., 2010). In the forward models, the ice model and the earth model are combined to compute the GIA velocities (Velicogna and Wahr 2006; Sasgen et al., 2007;) and the GIA vertical velocities can also be obtained by inversing other geodetic method, such as satellite altimetry and gravimetry technologies (Riva et al., 2009; Gunter et al., 2014). Differences in predictions of GIA for Antarctica persist due to the uncertainties of forward models in both the deglaciation history and Earth's rheology, but without adequate and accurate deglaciation history data, Earth structure models are greatly simplified in forward models, and the constraint data are poor in inverse models; thus, large differences in GIA persist for Antarctica. The GPS can record vertical land motion(VLM) and which has been used widely to constrain GIA uplift (Argus et al., 2014a; Peltier et al., 2015) or using a data-driven approach to directly solve for GIA (Wu et al., 2010). The actual GPS velocities are usually affected by two factors: CME and the ONM, therefore, when using the GPS velocity field to assess or extract the GIA signal, we must filter the CME and confirm the ONM. CME are thought to be related to the spatiotemporal distribution containing unmodeled signals and errors, including environmental loading effects (Atmospheric, non-tide, hydrology, etc.) and systematic errors (Dong et al., 2006). The detrimental effects of these errors could be effectively reduced after applying filtering.

Wdowinski et al. (1997) introduced Stacking to remove the CME of GPS time series in southern California. However, in spatial scale, we cannot describe the physical mechanism and effect of CME quantitatively. Dong et al. (2006）used principal component analysis (PCA) to analyze 5-year GPS time series in southern California. Since then, many researchers used widely PCA and modified PCA to remove the CME of GPS time series (Serpelloni et al., 2013; Shen et al., 2014; He et al., 2015; Li et al., 2015). However, CME derived PCA methods are usually considered to contain colored noise (Dong et al., 2006; Yuan et al., 2008). In addition, PCA method is based on second-order statistics and cannot take full advantage of higher-order statistics. Therefore, PCA filtering would result in contamination when applied to non-Gaussian GPS time series.

Relative to PCA, independent component analysis (ICA) can take full advantage of higher-order statistics to exploit the non-Gaussian features of the GPS time series (Hyvärinen & Oja 2000). Ming et al. (2017) adopted ICA for an investigation of 259 GPS stations in China. Li et al.（2019） compared the filtering results of Antarctica GPS residual time series derived from PCA and ICA. Considering the shortcomings of stacking and PCA filters, we apply ICA method to extract the CME of GNSS time series from Antarctica.

The noise model is another important factor which can affect the precision of velocity estimate. Previous studies shown that the GPS time series not only contain white noise (WN) but also colored noise, e.g., flicker noise (FN) and random walk noise (RW) (Zhang J et al.,1997 ; Mao A et al.,1999; Alvaro Santamaría-Gómez et al.,2011; Bogusz J and Klos A, 2016). If we ignored the effects of colored noise, the uncertainty of GPS velocity will be overestimated by a factor of 4 or even one order of magnitude higher than the signal amplitude (Yuan et al., 2008). For Antarctica which has a vast spatial area and complex terrain, it is not sufficient to reasonably and effectively model all GNSS station time series with only one noise model. In this paper, we adopted five noise models to confirm the ONM for the GPS time series in Antarctica: white noise plus power low noise (WN+PN), white noise plus random walk noise (WN+RW), white noise plus flicker noise (WN+FN), white noise plus power low noise plus random walk noise (WN+FN+RW), and white noise plus random walk noise plus generalized Gauss-Markov (WN+RW+GGM).

After regional filtering and confirming the ONM, we obtain the high-precision GPS velocity field, and 7 GIA models are assessed by the GPS velocity field: ICE-6G (VM5a) (Argus et al.，2014；Peltier et al.，2015),ICE-5G (VM2_L90) (Peltier et al.，2004：Argus et al.，2010),WANG (Wang et al.，2008),W12a (Whitehouse et al.，2012a、2012b),Geruo13 (Geruo et al.，2013),IJ05-R2 (Ivins et al.，2013)and Paulson07(Paulson et al.，2007)， The Geruo13 model has three submodels based on different truncation orders and Gauss filtering radii: (a) truncated to 100 order and no Gauss filtering; (b) truncated to 60 order and 200 km Gauss filtering; and (c) truncated to 40 order and 500 km Gauss filtering. The IJ05-R2 model has two submodels based on different parameters of the Earth model: (a) the lithosphere thickness is 65 km and the viscosity of the lower mantle is 1.5×1021 Pa.s; and (b) the lithosphere thickness is 115 km and the viscosity of the lower mantle is 4×1021 Pa.s. In this paper, we use Geruo13 (100 order) and IJR2-05 (65 km).

Martín-Español et al.(2016) used the elastic-corrected GPS vertical velocities in Antarctica over the period 2009-2014 to asses 8 GIA models, including forward and inverse methods, they found systematic underestimations of the GPS rates over specific regions characterized by low mantle viscosities and thin lithosphere. Liu et al. (2018) applied ICA and PCA for 53 GPS stations from 2010 to 2014, and used white noise plus power law (PL) noise model to estimate GPS velocities, after correction for elastic effects, they assessed the agreements of 4 GIA models and GPS vertical velocities. They found the agreements of the GPS observed velocities and GIA models are generally improved after the spatiotemporal filtering. Martín-Español et al.(2016) and Liu et al.(2018) used 53 GPS stations' velocities to assess the GIA models, but Martín-Español et al.(2016) without the filtering, and both them considered only one noise model, there is no uniform criterion that if we need to consider the effects of CME and noise models, therefore, a quantify study of the effects is needed in GPS velocities estimate and GIA assessment. In this paper, we used more than 79 stations with long time series (around 9 years) to achieve the confident velocity, then the influences of common mode error(CME) and 5 noise models on GPS accuracy were analyzed, finally, we assessed the application of GIA models in Antarctica.

The remainder of this paper is organized as follows. In section 2, the data processing and methods are briefly reviewed. The results of the processed GPS data and GIA model assessment are discussed in section 3. In section 4, we discuss the assessment results of different regions. The conclusions of our findings are presented in section 5.

2 Data processing and methods

2.1 GPS data

The GPS time series are downloaded from the Nevada Geodetic Laboratory(NGL). GPS time series were processed by GIPSY OASIS II software at the Jet Propulsion Laboratory (JPL), and the JPL's final orbit products were applied. Precise point positioning to ionospheric-free carrier phase and pseudorange data were used. The Global Mapping Function was applied to model tropospheric refractivity, with tropospheric wet zenith delay and horizontal gradients estimated as stochastic random-walk parameters every 5 min (Bar Sever et al., 1998). Coefficients were used to compute ocean loading for the site motion model, for which the FES2004 tidal model was applied, and ocean loading was also computed in the CM frame. Finally, ambiguity resolution was applied to double differences of the estimated one-way bias parameters (Blewitt, 1989) using the wide lane and phase bias (WLPB) method, which phase-connects individual stations to IGS stations in common view (Bertiger et al., 2010).The station coordinates were converted to the IGS08 frame using daily 7-parameter transformations.

Based on the distribution and integrity of the GPS time series, we selected 79 GPS stations with a time span from 8 February 2010 to 23 June 2018. The average proportion of missing data of our time series is 25.54%. Figure 1 shows the locations of the 79 GNSS stations in Antarctica. We used the third quartile criterion to removed abnormal data from the raw time series, then we subtracted these trends, annual and semiannual terms to form the residual time series by hector (the offsets estimation were based on the information http://geodesy.unr.edu/NGLStationPages/steps.txt.). For the missing values, we used the regularized expectation-maximization (RegEM) (Schneider 2001) algorithm to interpolate data and obtain the completed time series. We used the completed time series to performed an ICA regional filter. Then, we confirmed the ONM for all GPS time series based on AIC. Finally, we used the high-precision GPS velocity field to assess the 7 GIA models.

2.2 ICA filter

As presented by previous authors (Hyv ̈arinen & Oja 2000, Ming et al, 2017), if we want to get statistically independent components (ICs) from mixed-signals, we need to maximize the non-Gaussian characteristic of the output. Each observation $X_i(t) = [x_1(t), x_2(t), \cdots, x_n(t)]^T$ can be considered as a compound of the original signals $S_i(t)$,but the weights are different from each other. ICA method would get a separating matrix B, and then the signals $Y_i(t)$ and best estimates of S_i **(t).** When applied

ICA to GPS time series, each row vector x in X is the GPS coordinate series with trend and mean items removed. To remove CME using ICA, we first need to whiten the GPS time series using $Z = MX$ and $E(ZZ^T) = I$ (unit matrix), where M represents the whitened matrix and Z presents the whitened variables, and then we use ICA method to obtain a rotation matrix C, and maximize the non-Gaussian character of the projection $Y = C^T Z$. In this paper, we used the FastICA algorithm (Hyvärinen 1999; Hyvärinen & Oja 2000) to estimate the IC Y. The detailed description of the ICA filtering can be found in Liu et al.2018 and li et al. 2019.

First, we used a parallel analysis (PA) to confirm how many ICs are statistically significant. The PA analysis is a Monte Carlo-based simulation method which compares the observed eigenvalues with those simulated datasets. If the associated eigenvalue is larger than 99% of the distribution of eigenvalues derived from random data and the IC is retained (Peres-Neto and Jackson et al.， 2005). To investigate the influence of colored noise, we compared the simulation results using and without colored noise. The colored noise was generated by Fakenet (Agnew et al.2013). Figure 2 is the PA test results of ICs using and without colored noise data, from which we can see the first 7 eigenvalues are statistically significant, and colored noise has little influence, to avoid missing some information, we use the first 8 ICs to ICA filtering.

Figure 3 shows the spatial responses of IC1-IC8, from which we can conclude that IC2 has a uniform spatial coherence; IC4 and IC8 are neither completely random nor identical, but they exhibit obvious spatially uniform localized patterns or strong spatial coherence across the network; IC7 exhibits spatially uniform localized patterns in some areas, but the pattern is not entirely uniform, which we suppose is because the unmodeled signals, local effects, and other factors are not considered herein. Based on the spatial response, we used IC2, IC4, IC7, and IC8 to extract CME.

Figure 4 is the RegEM interpolated coordinate time series (the trend, annual and semiannual terms are removed) and raw time series of GMEZ before and after applying ICA filtering. Clearly, the scattering in the filtered time series is effectively reduced by the ICA filter, as the mean root mean square (RMS) values decrease from 6.41 mm to 4.46 mm, the maximum reduction in RMS value is 48.41%, the minimum value is 10.83%, and the mean value is 30.81%.

Figure 5 shows the RMS values of the residual time series before and after applying the ICA filters. The color bar is the the RMS reduction percentage; notably, the RMS values have a larger reduction in the SAP and the FRIS; the reductions in RMS values near the coast are smaller than those in the Antarctic interior regions.

We compared the environment loading and the ICA-extracted CME at site CAS1 (Figure 5), and the results show that CME amplitudes from ICs are not consistent with environment loading (atmospheric, non-tidal ocean, and continental water loading) the environment loading data can download from EOST Loading Service http://loading.ustrasbg.fr/displ_all.php. We checked the other sites and obtained the same results. We also computed the correlation between the CME from each IC and each loading model, and the results were poor. Furthermore, we computed the correlation between the sum of CMEs and the sum of loading displacements and obtained the same conclusion. Therefore, we think that the ICs of the CME cannot be explained by mass loadings and they are probably related to other non-geophysical errors, such as poorly modeled orbits or unmodeled tropospheric delay (Feng et al,2017).

2.3 AIC criterion and noise analysis

For the precision of GNSS coordinate time series, the noise model is one of the most important factors, the ONM will be quite different because of local effects among the stations in a network. It is not sufficient to reasonably and effectively model all GNSS station time series with only one noise model. We use the AIC (Akaike,1974; Schwarz,1978) to confirm the qualities of the selected noise models. The definition of the log-likelihood is as follows:

$$ln(L) = -\frac{1}{2}[Nln\ (2\pi)+lndet(C)+ \mathrm{r}^{\mathrm{T}}C^{-1}] \tag{1}$$

where N is the actual number of GPS observations (gaps do not contain), and r is the residual vector of the time series. The covariance matrix C is decomposed as follows:

$$C = \sigma^2 \bar{C}, \tag{2}$$

where $\bar{C}$ represents the sum of different noise models, and σ is the standard deviation of the conducting WN process, where σ is estimated from the residuals:

$$\sigma = \sqrt{\frac{\mathrm{r}^{\mathrm{T}}\bar{\mathrm{C}}^{-1}\mathrm{r}}{N}} \tag{3}$$

Then, the AIC can be defined as follows:

$$AIC = 2k + 2\,ln(L) \tag{4}$$

Because $detc\mathrm{A} = \mathrm{c}^{\mathrm{N}}\,detA$, the following formulation is implemented for the likelihood:

$$ln(L) = -\frac{1}{2}[Nln(2\pi) + lndet(\bar{\mathrm{C}}) + 2Nln(\sigma) + N]. \tag{5}$$

k is the sum of the parameters in the design matrix and the noise models. The minimum AIC value is the better model.

To determine the ONM for Antarctica, we use a combination of 5 noise models supplied by Hector (Bos et al., 2013) to analyze the 79 GNSS station time series based on AIC: WN+PN, WN+RW, WN+FN, WN+FN+RW, and WN+RW+GGM. The noise analysis results for the corresponding velocities listed in Table 1 show that the WN+FN ONM accounts for 22% (18 GPS stations), the WN+RW+GGM model accounts for 5.1% (4 GPS stations), and the WN+PN model accounts for 72.2% (57 GPS stations). Furthermore, we calculate the PN spectral index and find that most of the PN spectral index approximates the FN, which indicates that the PN essence is similar to that of FN in Antarctica.

3 Results

3.1 GPS velocity field

After applying AIC noise analysis and ICA filters, we obtain a high-precision GPS velocity field, and then, we compare the velocity changes with the raw GPS velocity. The result shows that the maximum difference is up to 1.2 mm yr^{-1} (WWAY), the mean difference is 0.2 mm yr^{-1}, and 21 % (17 stations) of the velocities are greater than ±0.4 mm yr^{-1}. We exclude 9 stations that are inappropriate percentage statistics: FIE0, BUMS, MAW1, PECE, OHI2, STEW, VESL, MCM4, and HOOZ (processed GPS velocities are far greater than the raw velocities or the velocity directions are changed before and after applying AIC and ICA). We calculate the percentage of velocities that vary relative to raw GPS velocities, the maximum variety of processed velocities is 80.22 %(ABBZ, which has a very small velocity magnitude), and the mean variety is 11.39 %. We find that the maximum velocity variety is up to 0.9 mm yr^{-1}, and the mean variety is 0.6 mm yr^{-1} at the remaining 9 stations. Considering the elastic and GIA magnitudes, we cannot ignore these effects.

Figure 7 is the GPS velocity field after applying noise analysis and the AIC filter to Antarctica. The overall trend is upward. INMN has a maximum uplift velocity of 32.6 mm yr^{-1}, a mean velocity of 3.3 mm yr^{-1} (TOMO were removed because of some abnormal variations) (Martin-Espnol et al., 2016). Due to the lower upper mantle viscosity and mass loss caused by the collapse of the Larsen-B Ice Shelf (Nield et al., 2014), the north Antarctic Peninsula (NAP) mean uplift velocities (5.8 mm yr^{-1}) are larger than those of the SAP (3.7 mm yr^{-1}). The FRIS mean uplift velocities (4.7 mm yr^{-1}) are larger than those of the Ross Ice Shelf (ROSS, 0.74 mm yr^{-1}). The Amundsen Sea Embayment (ASE) has a mean uplift velocity of up to 13.0 mm yr^{-1}, which is the maximum amount of ice mass loss (Groh et al., 2012;Barletta et al.,2018）. The most stable region is the East Antarctic (EA) coast, where the mean uplift velocity is only 0.1 mm yr^{-1}.

The GPS data time span also has an important effect on velocity estimation, such as CAPF, located in NAP, and the vertical velocity is estimated at 15.0 ±8.4 mm yr^{-1} in Argus et al. (2014) based on approximately two years of GPS data, which is far greater than our estimated value of 4.1 ±0.3 mm yr^{-1} in this study. ROB4 is located on the west coast of the Ross Ice Shelf, and the vertical velocity is estimated at 1.1 ±0.2 mm yr^{-1}, which is similar to the 2.2 ±3.2 mm yr^{-1} estimated in Argus et al. (2014) based on approximately six years of GPS data and is dramatically different from the 7.5 ±2.6 mm yr^{-1} estimated in Thomas et al. (2011) based on 558 days of GPS data. These differences show that the GPS data time span plays an important role in the velocity estimation, and the longer the time span is, the more reliable the velocity estimation will be.

3.2. Elastic correction

In Antarctica, the GPS uplift velocities are dominated by the elastic deformation due to present ice mass loading and GIA. Riva et al. (2017) shown that the elastic response has a long wavelength influence in Antarctica; they used mass loss from glaciers, ice sheets, Greenland and Antarctic ice sheets in 1902 and 2014 to determine solid Earth deformation at regional and far fields. Based on the result in Riva et al. (2017), we calculated uplift velocities at 79 GPS sites. Figure 8 shows the GPS elastic velocities in Antarctica; the Antarctic Peninsula and ASE regions have larger elastic velocities and mean magnitudes of 2.2 mm yr^{-1} and 1.0 mm yr^{-1}, respectively. The FRIS and ROSS regions have smaller elastic velocities, while the EA has a negative elastic response. Clearly, the estimated GIA uplift rates would be significantly contaminated and in some areas dominated by neglecting the elastic response. When applying the elastic deformation correction, we consider GPS vertical velocities are mainly caused by GIA. We use the corrected GPS velocities to assess 7 GIA models: ICE-6G (VM5a), ICE-5G (VM2), WANG (CE-4G+RF3L20, β=0.4), W12a, Geruo13, IJ-05R2, and Paulson.

3.3. GIA assessment

To explore the application of GIA models in different regions, we divide Antarctica into 6 subregions（Sasgen et al. , 2013；Martin et al., 2016) and show these subregions in figure 9. The station information is indexed in Table S1.

Notably, the reference frame origin of the GIA model is the center of mass (CM) of the solid Earth (CE), while the GPS velocities are estimated in the ITRF2008 reference frame, whose origin is the CM of the total Earth system. Argus et al. (2014) thought the velocities between CM and CE caused by GIA are very small, but the velocities caused by the modern ice mass loss are more significant. If the ice loss in Greenland was 200 Gt yr^{-1} and there is no ice loss in other areas, then the velocity is approximately 0.2 mm yr^{-1}, Schumacher et al. (2018) found that the effect of the frame origin transformation on the GPS uplift rates is very small (less than ±0.2 $mmyr^{-1}$).The above corrections are much smaller than the uncertainty of the GIA models and GPS vertical velocities, and therefore, the impact of these corrections can be ignored in this study.

Figure 10 is the predicted uplift velocities of 7 GIA models, and the maximum, minimum, mean, and RMS values of the uplift velocities are listed in Table 2. From Fig.8, we can see that SAP, ASE, ROSS, and FRIS have larger uplift velocities, which may be caused by the most ice mass loss since the LGM and the rapid response of the solid Earth （Mart ń-Espanol et al., 2016）. The vertical velocities predicted over the West Antarctica (WA) are bigger than those in EA basins, while the vertical velocities have a smaller values along coastal EAs, and there are different sizes subsidence areas in the interior across solutions, which may be because of the low upper mantle viscosities and higher values in EAs (An et al., 2015; vander Wal et al.,2015). Because of lacking ice history data in GIA models, EAs has a small variability between solutions (Mart ń-Espanol et al., 2016). The spatial variability in all GIA models is larger than the GIA signal itself in many cases, especially in the interior areas of EAs where the mean GIA velocities are small. We find that the western margin of the Ross Ice Shelf, the ASE sector, the FRIS, and the Antarctic Peninsula(AP) have maximum variability.

The predictions of the ICE-5G, Geruo13 and Paulson models are quite similar in terms of spatial distribution, which may be caused by the same ice model ICE-5G employed in the GIA modeling. The predictions are quite different among the ICE-6G, WANG, IJ05-R2 and W12a models, which employed different ice models, indicating that the ice models play a major role in the predictions of GIA models. Earth models have much less effect than ice models in GIA modeling, which may be related to the unconsidered lateral variation in mantle viscosity (Ivins et al., 2005). ICE-6G, W12a and IJ05-R2 employed the new ice models; they have a similar distribution patterns of maximum uplift velocities and an obvious submerged trend in the interiors, while the magnitudes of the IJ05-R2 uplift velocities are much less than those of ICE-6G and W12a. From Table 2, we can see that the IJ05-R2 velocities have the minimum standard deviation (std). The distribution pattern of the WANG model differs greatly from that of the other 6 GIA models; the pattern shows larger uplift velocities in the NAP and Enderby Land. All GIA models have maximum uplift velocities in the nearby ROSS and FRIS regions. ICE-6G has a peak descent velocity in the South Weddell Sea of approximately -2.2 mm yr^{-1}. The W12a has a peak descent velocity of approximately -6.1 mm yr^{-1} near Coats Land; IJR5-R2 has no obvious peak descent velocity, which means that there is greater uncertainty in some or all 3 GIA models, and systematic differences are also likely.

Generally, the Antarctic GIA models still have great uncertainty with a lack of adequately accurate constraint data. As presented by Mart ń-Espanol et al. 2016, we use the weighted mean (WM), weighted root mean square (WRMS) and median values to evaluate the consistency between GPS vertical velocities and GIA model velocities. WM and WRMS are defined by formulas (6) and (7):

$$\mathrm{WM}=\frac{\sum_{i=1}^{79}(p_i-O_i)w_i}{\sum_{i=1}^{79}w_i} \tag{6}$$

$$\mathrm{WRMS}=\sqrt{\frac{\sum_{i=1}^{79}(P_i-O_i)^2 w_i}{\sum_{i=1}^{79}w_i}} \tag{7}$$

where P_i and O_i are the GIA-modeled and GPS-observed velocities, and W_i is the weight factor obtained by GPS measurement errors at each station:

$$w_i=\frac{1}{c_i(\sigma_i^{GPS})^2}\; i=1,\cdots 79 \tag{8}$$

where σ_i represents the error at GPS station and c_i is calculated as follows:

$$C_i=\sum_{j=1}^{79}\exp\left(\frac{-d_{ij}}{I}\right) \tag{9}$$

x is distance matrix and d_{ij} is the ith, jth value of the x relative to the 79 GPS locations, in order to deweight the sites that are near to other sites, we used the scale parameter I. Similar to Mart ń-Espanol et al. 2016, we also assume I = 250 km. The WM and WRMS results before and after applying the ICA and noise analysis are listed in Tables 3 and 4, respectively (* indicates the results of applying the ICA and noise analysis).

Table 3 shows the WMs of Antarctica and the subregions. After applying the ICA filter and noise analysis, the WM values of all GIA models are reduced in ASE. The ICE-6G, ICE-5G, WANG, W12a, and Geruo13 models are also reduced near FRIS. The WM values of most GIAs in other regions are increased. For all 79 stations, the WM of the residuals between the ICE-6G, WANG, W12a, and Paulson07 models and observed uplift velocities are increased. We think that the consistency between the raw GPS velocities and the 4 GIA model uplift velocities are overly optimistic, the two have poor consistency. The WM values of ICE-5G and Geruo13 are from negative to positive, which also indicates that the effects of the regional filter and the noise model are not negligible.

Table 4 shows the WRMSs of Antarctica and the subregions. The WRMS of the Antarctica peninsula (AP) and ASE are increased after applying the ICA filter and noise analysis, which we infer due to the local effects or inaccurate elastic model.

In some regions with obvious GIA effects, such as the ROSS and FRIS regions (Argus et al., 2014; Martin et al., 2016), the WRMSs are effectively reduced. The WRMSs of all of Antarctica are reduced, which means that raw GPS velocities are affected by local effects. After applying the ICA filter and noise analysis, the local effects are depressed. In some regions with relatively good consistency between GPS observed velocities and GIA model predicted velocities, the consistency becomes better.

Figure 11 shows the summary statistics of WM and WRMS and the median values of residuals (GPS velocities with ICA filter applied and the ONM and GIA model predicted velocities). The WM of GPS and IJ05-R2 is -0.7 mm yr^{-1}, which indicates that the predicted velocities of IJ05-R2 are systematically smaller than GPS observed velocities. The WM of the other 6 GIA models range from 0.3 mm yr^{-1} to 2.1 mm yr^{-1}, which means that the model predicted velocities are systematically larger than the GPS observed velocities. The WM of ICE-5G and Geruo13 are relatively small, which indicates that the two models are unbiased with GPS velocities. WANG has the maximum median and WM values. ICE-6G has the minimum WRMS, which we infer to be because the ICE-6G employed GPS data as a constraint (Argus et al., 2014).

4. Discussion

To evaluate the GIA models applicability in Antarctica, the estimates velocities and observed vertical velocities by an independent set of 78 GPS stations were compared. Figure12 is the discrepancies between the GIA velocities and GPS uplift rates at each GPS site; then, we perform the regional analysis and interpret the GIA uplift rates.

ASE: ASE is undergoing a large ice mass loss, and the GIA contribution and upper mantle have significant effects on gravity-derived ice mass variation estimates and ice-sheet stability, respectively. Moreover, the viscosity under ASE is likely underestimated (4×10^{18} pascal-second) and could shorten the GIA response time scale by decades up to a century (Barletta et al.2018). The GIA signal in low mantle viscosity regions mainly reflects significant decadal-to-centennial ice load change, and most forward models do not account for such signals; therefore, the GIA signal of forward models are substantially less than that of inverse solutions. The difference between new GIA models and GPS velocity results (after elastic correction) were compared, and the results show that important differences still remain in West Antarctica, especially in ASE and NAP (Whitehouse et al. 2019).Figure 12 shows the difference between the GPS and GIA velocities at each GPS site, and the matching results are the worst in the ASE. The GPS uplift velocities along the ASE coast have larger differences, ranging from -1.8 mm yr^{-1} (THUR) to 27.3 mm yr^{-1} (BERP). All GIA model predicted velocities are systematically underestimated at the INMN, BERP, and BACK stations. ICE-6G has a maximum uplift velocity of approximately 7 mm yr^{-1},which has an intermediate upper mantle value among most GIA models and predicts the largest present-day uplift velocity in ASE (Barletta et al.2018), The next is W12a, which has an uplift velocity of approximately 5 mm yr^{-1}, and the other models are within 2 mm yr^{-1}. From Table 4, we know that the ASE region has the maximum WRMS, and the largest discrepancy between the GPS and GIA models is greater than 20 mm yr^{-1} (INMN). Removing the INMN and BERP stations, which have large uplift velocities, reduces the WRMS values to 7.0 mm yr^{-1}, 5.9 mm yr^{-1}, 5.6 mm yr^{-1}, 5.9 mm yr^{-1}, 5.8 mm yr^{-1}, 5.5 mm yr^{-1}, and 5.6 mm yr^{-1}.

Seismic evidence reveals there is a very low upper mantle viscosity, about 10^{18} Pa s in this area (An et al., 2015; Heeszel et al., 2016), that could cause a fast response to ice mass changes at a smaller scale (Martin et al., 2016). Zhang et al. (2017) also revealed that ASE is one of the regions that has experienced the most significant ice mass loss and most significant elastic vertical crustal deformation. The stations BACK, BERP and TOMO are all located in the Pine Island Bay region, and recent studies indicate that fast ice mass loss occurs in both the Pine Island Glacier and Thwaites Glacier in this region.

ROSS: King et al. (2012) showed that the GIA signal in the Ross Ice Shelf should be close to zero by examining GRACE data. The GRACE signal should be dominated by GIA and small ocean mass changes. Nield et al. (2016) predicted the uplift velocity across Siple Coast are more than 4 yr mm-1, and GIA vertical velocities are small over the Ross Ice Shelf and Siple Coast only when upper mantle viscosities are 0.5-1.0 $\times 10^{20}$ Pa s, which is compatible with King et al. (2012), and they also showed that Late Holocene ice load changes may have a dominant influence on defining the present uplift of this region.

In our study, the GPS velocities are from -2.3 mm yr^{-1} to 7.0 mm yr^{-1} in the ROSS region, and the mean velocity is approximately 0.7 mm yr^{-1}. All GIA model predicted velocities are consistent with the GPS observed velocities. Except for the IJ05-R2 underestimation by 0.8 mm yr^{-1}, the other models overestimated the velocities in this region by approximately 1.0 mm yr^{-1} ~ 2.2 mm yr^{-1}. The W12a model has the maximum WRMS and overestimates by approximately 2.3 mm yr^{-1}, which suggests that the ice in W12a model was too much in LGM, or the upper mantle viscosity was too large (Martin et al., 2016).

AP: The GPS vertical velocities in the Antarctic Peninsula are generally larger than the predictions of all GIA models. This study's uplift estimate of the FONP station is 11.9 mm yr^{-1}, while the mean GIA prediction is 2.0 mm yr^{-1}. One possible cause for such a difference is the crustal elastic response to the modern ice mass change. The Prince Gustav Ice Shelf and Larsen-A Ice Shelf collapsed in 1995. The neighboring Larsen-B Ice Shelf partially collapsed in 2002 and is quickly weakening and likely to completely disintegrate before the end of the decade. Ice shelves are the gatekeepers of glaciers flowing from Antarctica toward the ocean (Martin et al., 2016). Without ice shelves, the glacial ice enters the ocean faster and accelerates the pace of global sea level rise. Thomas et al. (2011) found that the uplift velocities of the stations in this region increased obviously after the collapse of the Larsen-B Ice Shelf; for example, the velocity of PALM was 0.1 mm yr^{-1} before 2002 and reached 8.8 mm yr^{-1} after 2002. Except for WANG overestimating the velocities by 2.3 mm yr^{-1}, the GIA models generally underestimated the velocities by more than 1.07 mm yr^{-1}~4.4 mm yr^{-1} in the NAP. ICE-6G values are relatively consistent with the GPS velocities. The GPS vertical velocities in the NAP are generally larger than those in the SAP, which agrees with Wolstencroft et al. (2015), indicating a moderately low upper mantle viscosity in SAP, even though not as low as NAP. Nield et al. (2014) used a high-resolution ice elevation change dataset to compute the elastic correction in NAP, and a comparison of the GPS results and modelled uplift indicates upper mantle viscosities of between 6×1017 and 2×1018 in NAP (as Zhao et al. 2016). Moreover, the results show that the lithospheric thickness and upper mantle viscosity are much lower than that in the previous study. ” Zhao et al. (2016) also found a higher viscosity of the Earth in the SAP than previously reported in the NAP, and the viscosity changes in north-south gradient can be an order of magnitude over 500 km.

FRIS: FRIS is near the Weddell Sea Embayment, the crustal thickness in the transition between EAs and WAs and the mantle viscosity are moderate (An et al., 2015; Heeszel et al., 2016). The mean GPS uplift velocity is 4.3 mm yr^{-1}, the uplift velocities are underestimated by the ICE-5G, Geruo13, and IJ05-R2 models by 3.49 mm yr^{-1}, 3.5 mm yr^{-1} and 0.9 mm yr^{-1}, respectively, and overestimated by 0.4 mm yr^{-1} ~1.7 mm yr^{-1} by the other models. The matching results between the GPS and GIA are better overall, so we think that the uplift is mainly caused by the GIA in this region, which agrees with the findings of (Arguset al.,2014; Martin et al.,2016).

EAs: EA is characterized by higher upper mantle viscosity than West Antarctica, with exceptionally low upper mantle viscosity on the order of 1018 to 1019 Pa s beneath some regions of West Antarctica. Across EA, spatial variations in Earth rheology are currently poorly constrained (Whitehouse et al. 2019). Our GPS vertical velocities along the EAs coast range from -1.9 mm yr^{-1} ~2.5 mm yr^{-1} and are smaller than those in WAs The GIA model velocities agree with the GPS velocities. The uplift velocities are underestimated by ICE-5G and Geruo13 by approximately 0.5 mm yr^{-1} and 0.5 mm yr^{-1}, respectively, and overestimated by the other models by 0.4 mm yr^{-1} ~1.7 mm yr^{-1}. The basement of EAs is an ancient craton, and the geological structure is very stable, so there is no significant geological activity occurring in this region. The vertical movements along the EAs coast are all nonsignificant, showing the effects of the GIA or recent ice and snow accumulations to be small. GRACE gravity data from 2009-2013 show that the coast of Queen Maud Land in EAs accumulated ice and snow at a rate of 150 Gt yr^{-1} (Argus et al., 2014). The precipitation data from 2009-2012 also measure fast accumulation, but the accumulation from 1980-2008 is approximately zero, indicating that the recent ice and snow accumulation is anomalous and represents interannual variations (Boening et al., 2012). Overall, there is no significant geological activity in EAs, and the effects of the GIA and ice mass loading are small in this region.

5. Conclusions

High-precision GPS data are an effective approach for studying regional crustal displacements. Studying the regional crustal displacement in Antarctica has important value as a reference for the formation and evolution of global plate tectonics in addition to creating and maintaining reference frames and monitoring the dynamics of ice and snow in polar regions. For the regions of Antarctica with complex terrain, we removed the CME of the residual time series by ICA filtering of the time series recorded at 79 GNSS stations in Antarctica, and then, the AIC is used to determine the ONM. Finally, we used high-precision GPS data to assess the 7 GIA models. The results are as follows:

1. After applying an AIC noise analysis and the ICA filter, the maximum difference is up to 1.2 mm yr^{-1}, the mean difference is 0.2 mm yr^{-1}, 21 % (17 stations) of the velocities are greater than ±0.4 mm yr^{-1}, the maximum variety of processed velocities is 80.22 %, and the mean variety is 11.39 %.
2. After applying the ICA filter and noise analysis, the WM values of all GIA models are reduced in ASE, and the ICE-6G, ICE-5G, WANG, W12a, and Geruo13 models are also reduced near FRIS; the WM values are increased for most of the GIA in other regions; for all 79 stations, the WMs of residuals between the ICE-6G, WANG, W12a, and Paulson07 models

and observed uplift velocities are increased. The WRMS of AP and ASE are increased after applying the ICA filter and noise analysis; in some regions with obvious GIA effects, such as the ROSS and FRIS regions, the WRMSs are effectively reduced. The WRMSs of all of Antarctica are reduced, which means that the raw GPS velocities are affected by local effects. After applying the ICA filter and noise analysis, the local effects are depressed; in some regions with relatively good consistency between the GPS observed velocities and GIA model predicted velocities, the consistency becomes better.

3. The predicted velocities of IJ05-R2 are systematically smaller than the GPS observed velocities; the other 6 GIA model predicted velocities are systematically larger than the GPS observed velocities. The WMs of ICE-5G and Geruo13 are relatively small. WANG has the maximum median and WM values. ICE-6G has the minimum WRMS. Because the upper mantle viscosities in the NAP are lower than in the SAP, the GPS velocities shows the largest vertical deformation in the NAP than SAP. In the FRIS ice shelves, the observed GPS velocities and the predicted GIA model velocities are consistent. In EA, the vertical motion is nonsignificant, and the GIA and ice loading have a small impact in this area.

References

Wang, H., Wu, P., Wal, W. V. D.: Using postglacial sea level, crustal velocities and gravity-rate-of-change to constrain the influence of thermal effects on mantle lateral heterogeneities[J]. Journal of Geodynamics, 2008, 46(3-5):0-117. doi: 10.1016/j.jog.2008.03.003

Ivins, E. R., James, T. S., Wahr, J., Schrama, E., Landerer,F.W., Simon K.M.:Antarctic contribution to sea level rise observed by GRACE with improved GIA correction. Journal of Geophysical Research: Solid Earth, 118(6): 3126-3141, doi: 10.1002/jgrb.50208,2013.

Argus, D.F., Blewitt, G., Peltier, W.: Rise of the Ellsworth mountains and parts of the East Antarctic coast observed with GNSS. Geophys. Res. Lett. 38. doi: 10.1029/2011GL048025,2010.

Hao, K.E., Fei, L.I., Sheng-Kai, Z., Chao, M.A., Ai-Xue,W.:The determination of absolute sea level changes of the Antarctic coast tidal gauges from 1994 to 2014 and its analysis. Chin. J. Geophys. 59, 3202–3210, doi: 10.6038/cjg20160906,2016.

Peltier, W.R.: Global glacial isostasy and the surface of the ice-age Earth: the ICE-5G (VM2) model and GRACE, Ann. Rev. Earth planet. Sci., 32, 111–149,doi:10.1146/annurev.earth.32.082503.144359, 2004.

Riva, R. E. M., B. C. Gunter.,T. J. Urban., B. L. a., Vermeersen, R. C., Lindenbergh, M. M., Helsen, J. L. Bamber, R. S. W., vande Wal, M. R., van den, Broeke., B. E. Schutz.: Glacial isostatic adjustment over Antarctica from combined ICESatand GRACE satellite data, Earth Planet. Sci. Lett., 288(3–4), 516–523, doi: 10.1016/j.epsl.2009.10.013,2009.

King, M.A. et al., , Altamimi, Z., Boehm, J. , Bos, M. , Dach, R . , Elosegui, P., Fund, F., Hernandez-Pajares, M., Lavallee, D., Cerveira, PJM., Penna, N., Riva, REM. , Steigenberger, P., van Dam, T. , Vittuari, L ., Williams, S., Willis, P.: Improved constraints on models of glacial isostatic adjustment: a review of the contribution of ground-based geodetic observations, Surv. Geophys., 31(5), 465–507. doi: 10.1007/s10712-010-9100-4,2010.

Sasgen, I.,Z. Martinec0., K. Fleming.: Regional ice-mass changes and glacial-isostatic adjustment in Antarctica from GRACE, Earth Planet. Sci. Lett., 264(3), 391–401. doi: 10.1016/j.epsl.2007.09.029,2007.

Velicogna, I., J. Wahr.: Measurements of time-variable gravity show mass loss in Antarctica, Science, 311(5768), 1754–1756,doi:10.1126/science.1123785,2006.

Gunter, B. C., O. Didova., R. E. M. Riva. , S. R. M. Getenberg. , J. T. M. Lenaerts. , M. A. King. , M. R. van den Broeke, and T. Urban.: Empirical estimation of present-day antarctic glacial isostatic adjustment and ice mass change, The Cryosphere, 8, 743–760. DOI: 10.5194/tc-8-743-2014,2014.

Whitehouse, P.L., Bentley, M.J., Milne, G.A., King, M.A., Thomas, I.D.: A new glacial isostatic adjustment model for Antarctica: calibrated and tested using observations of relative sea-level change and present-day uplift rates, Geophys. J. Int., 190, 1464–1482. DOI: 10.1111/j.1365-246X.2012.05557.x,2012.

Peltier, W.R., Argus, D.F., Drummond, R.: Space geodesy constrains ice-age terminal deglaciation: The global ICE-6G C (VM5a) model, J. geophys. Res., 120, 450–487. DOI: 10.1002/2014JB011176,2015.

Wu, XP. , Heflin, MB. , Schotman, H., Vermeersen, BLA. , Dong, D.A. , Gross, R.S. , Ivins, E.R. , Moore, A., Owen, S.E.: Simultaneous estimation of global present-day water transport and glacial isostatic adjustment, Nat. Geosci., 3, 642–646. DOI: 10.1038/NGEO938,2010.

Dong, D., Fang, P., Bock, Y., Webb, F., Prawirodirdjo, L., Kedar, S.: Spatiotemporal filtering using principal component analysis and karhunen-loeve expansion approaches for regional gps network analysis. J Geophys Res Solid Earth, 111 (B3),1-16, doi: 10.1029/2005JB003806,2006.

Wdowinski, S., Bock, Y., Zhang, J.: Southern California permanent GNSS geodetic arrary: spatial filtering of daily positions for estimating coseismic and postseismic displacements induced by the 1992 Landers earthquake. J Geophys Res. 102, 18057–18070, doi:10.1029/97JB01379,1997.

Serpelloni, E., Faccenna, C.,Spada, G., Dong, D. , Williams, S.: Vertical GPS ground motion rates in the Euro-Mediterranean region: new evidence of velocity gradients at different spatial scales along the Nubia-Eurasia plate boundary, J. geophys. Res., 118(11), 6003–6024.DOI：10.1002/2013JB010102,2013.

Shen, Y., Li, W., Xu, G., Li, B.: Spatiotemporal filtering of regional GNSS network’s position time series with missing data using principle component analysis, J. Geodyn., 88, 1–12, doi:10.1007/s00190-013-0663-y,2014.

He, X., Hua, X., Yu, K., Xuan, W., Lu, T., Zhang, W., Chen, X.: Accuracy enhancement of GPS time series using principal component analysis and block spatial filtering, Adv. Space Res., 55, 1316–1327, doi: 10.1016/j.asr.2014.12.016, 2015.

Li, W., Shen, Y., Li, B.: Weighted spatiotemporal filtering using principal component analysis for analyzing regional GNSS position time series, Acta Geod. Geophys. 50, 419–436,doi: 10.1007/s40328-015-0100-1,2015.

Yuan, L., Ding, X., Chen, W., Guo, Z., Chen, S., Hong, B., Zhou, J.: Characteristics of daily position time series from the hong kong GNSS fiducial network. Chinese J. Geophys. 51, 418-420,doi:10.1002/cjg2.1292, 2008.

Liu, B., Matt, K., Wujiao, D.: Common mode error in Antarctic GPS coordinate time series on its effect on bedrock-uplift estimates. Geophys. J. Int. doi:10.1093/gji/ggy217,2018.

Hyvärinen, A., Karhunen, J., Oja, E.: Independent component analysis. Wiley, New York, doi:10.1007/978-1-4614-6170-8_147, 2001.

Ming, F., Yang, Y., Zeng, A., Zhao, B.: Spatiotemporal filtering for regional GNSS network in China using independent component analysis. J Geod. 91:419–440 , doi: 10.1007/s00190-016-0973-y,2017.

Li W., Li F.,Zhang S.,Lei J., Zhang Q., Yuan L.: Spatiotemporal Filtering and Noise Analysis for Regional GNSS Network in Antarctica Using Independent Component Analysis. Remote Sens. 11(4), 386, https://doi.org/10.3390/rs11040386,2019.

Zhang, J., Bock, Y., Johnson, H. Fang, P., Williams, S.D.P.,Genrich,J.,Wdowinski,S.,Behr,J.: Southern California permanent GPS geodetic array: Error analysis of daily position estimates and site velocities. J Geophys Res Solid Earth 102, 18035–18055, doi: 10.1029/97JB01380,1997.

Mao, A., Harrison, C.G.A., Dixon, T.H.: Noise in GPS coordinate time series. Geophys. J. Int. 104, 2797-2816, doi: 10.1029/1998jb900033 ,1999.

Alvaro Santamaría-Gómez, Marie-Noëlle Bouin, Collilieux, X. , Guy Wöppelmann: Correlated errors in gps position time series: implications for velocity estimates. Journal of Geophysical Research: Solid Earth, 116.DOI: 10.1029/2010JB007701,2011.

Bogusz J , Klos A . On the significance of periodic signals in noise analysis of GPS station coordinates time series. GPS Solutions, 20(4):655-664. DOI: 10.1007/s10291-015-0478-9. 2016.

Argus D. F., Peltier W. R., Drummond R., Moore, A.W.: The Antarctica component of postglacial rebound model ICE-6G_C (VM5a) based on GPS positioning, exposure age dating of ice thicknesses, and relative sea level histories. Geophysical Journal International, 198(1): 537-563. DOI: 10.1093/gji/ggu140 ,2014.

Peltier, W.R., Argus, D. F., Drummond R.: Space geodesy constrains ice age terminal deglaciation: The global ICE-6G_C (VM5a) model. Journal of Geophysical Research: Solid Earth, 120(1): 450-487.DOI：10.1002/2014JB011176 ,2015.

Whitehouse, P. L., Bentley, M. J., Le Brocq, A. M.: A deglacial model for Antarctica: geological constraints and glaciological modelling as a basis for a new model of Antarctic glacial isostatic adjustment[J]. Quaternary Science Reviews, 32: 1-24.DOI：10.1016/j.quascirev.2011.11.016 ,2012a.

Whitehouse, P. L., Bentley, M. J., Milne, G. A., Matt, A.K., Thomas L.D.: A new glacial isostatic adjustment model for Antarctica: calibrated and tested using observations of relative sea-level change and present-day uplift rates. Geophysical Journal International, 190(3): 1464-1482. doi.org/10.1111/j.1365-246X.2012.05557.x,2012b.

A.G., Wahr, J., Zhong, S.: Computations of the viscoelastic response of a 3-D compressible Earth to surface loading: an application to Glacial Isostatic Adjustment in Antarctica and Canada. Geophysical Journal International, 192(2): 557-572.DOI：10.1093/gji/ggs030,2013.

Ivins, E. R., James, T. S. Wahr, J. Schrama, E.J.O. , Landerer, F.W. , Simon, K.M.: Antarctic contribution to sea level rise observed by GRACE with improved GIA correction. Journal of Geophysical Research: Solid Earth, 118(6): 3126-3141.

DOI: 10.1002/jgrb.50208,2013.

Paulson, A., Zhong, S., Wahr, J.: Inference of mantle viscosity from GRACE and relative sea level data. Geophysical Journal International, 171(2): 497-508.DOI：10.1111/j.1365-246X.2007.03556.x, 2007.

Bar-Sever, Y. E., Kroger, P. M., Borjesson, J. A.: Estimating horizontal gradients of tropospheric path delay with a single gps receiver. Journal of Geophysical Research,103(B3), 5019. DOI：10.1029/97jb03534 ,1998.

BLEWITT G. Carrier Phase Ambiguity Resolution for the Global Positioning System Applied to Geodetic Baselines up to 2000 km. Journal of Geophysical Research, 94(B8): 187-203. DOI:10.1029/jb094ib08p10187, 1989.

Bertiger, W., Desai, S. D. , Haines, B. , Harvey, N. , Moore, A. W. , Owen, S. , Weiss J.P.: Single receiver phase ambiguity resolution with gps data. Journal of Geodesy, 84(5), 327-337.DOI：10.1007/s00190-010-0371-9,2010.

Schneider, T.: Analysis of Incomplete Climate Data：Estimation of Mean Values and Covariance Matrices and Imputation of Missing Values . J. Climate, American Meteorological Society. 14, 853—871, doi: 10.1175/1520-0442(2001)014<0853:AOICDE>2.0.CO,2,2001.

Hyv ̈arinen, A.: Fast and robust fixed-point algorithms for independent component analysis, IEEE Trans. Neural Netw. 10(3), 626–634.DOI：10.1109/72.761722,1999.

Hyvärinen, A., Karhunen, J., Oja, E.: Independent component analysis. Wiley, New York, doi:10.1007/978-1-4614-6170-8_147,2001.

Peres-Neto, P.R., Jackson, D.A. Somers K M.: How Many Principal Components? Stopping Rules for determining the Number of Non-trival Axes Revisited. Computational Statistics & Data Analysis.. 48, 974–997, doi: 10.1016/j.csda.2004.06.015,2005.

Agnew, D. C. (2013), Realistic simulations of geodetic network data: The Fakenet package,, Seismol. Res. Lett., 84, 426–432, doi:10.1785/gssrl.84.3.426.

Bos, M.S., Fernandes, R.M.S., Williams, S.D.P., Bastos, L.: Fast error analysis of continuous gnss observations with missing data. J. Geod. 87, 351–360, doi:10.1007/s00190-012-0605-0,2013.

Akaike, H. A new look at the statistical model identification. IEEE Transactions on Automatic Control, 19(6):716–723. DOI: 10.1109/TAC.1974.1100705.1974.

Schwarz, G. Estimating the Dimension of a Model. The Annals of Statistics,6(2):461–464.DOI:10.1214/aos/1176344136.1978.

Mart ́ın-Espa ̃nol, A., King, M.A., Zammit-Mangion, A., Andrews, S.B.,Moore, P., Bamber, J.L.: An assessment of forward and inverse GIA solutions for Antarctica, J. geophys. Res. 121(9), 6947–6965.DOI: 10.1002/2016JB013154,2016.

Nield, G. A., V. R. Barletta, A. Bordoni, M. A. King, P. L. Whitehouse, P. J. Clarke, E. Domack, T. A. Scambos, and E. Berthier.: Rapid bedrock uplift in the Antarctic Peninsula explained by viscoelastic response to recent ice unloading, Earth Planet. Sci. Lett., 397, 32–41,doi:10.1016/j.epsl. 2014.04.019, 2014.

Groh, A., H.,Ewert, M., Scheinert, M., Fritsche, A., Ru ke, A., Richter, R., Rosenau and R. Dietrich.: An investigation of glacial isostatic adjustment over the Amundsen Sea sector, West Antarctica, Global Planet. Change, 98–99, 45–53.DOI：

10.1016/j.gloplacha.2012.08.001, 2012.

Thomas,I.D., King,M.A. , Bentley,M.J. , Whitehouse,P.L. , Penna,N.T. , Williams,S.D.P. , Riva,R.E.M. , Lavallee, D.A. , Clarke, P.J., King, E.C. , Hindmarsh, R.C.A. Koivula, H.: Widespread low rates of Antarctic glacial isostatic adjustment revealed by GPS observations, Geophys. Res. Lett., 38, L22302, doi:10.1029/2011GL049277,2011.

Riva, R.E.M.,Frederikse, T., King, M.A., Marzeion, B. , van den Broeke, M.R.: Brief communication: the global signature of post-1900 land ice wastage on vertical land motion, The Cryosphere, 11, 1327–1332.DOI：10.5194/tc-2016-274,2017.

Sasgen, I.,H. Konrad,E. R. Ivins,M. R. van den Broeke, J. L. Bamber, Z. Martinec, V. Klemann.: Antarctic ice-mass balance 2002 to 2011: regional re-analysis of GRACE satellite gravimetry measurements with improved estimate of glacial-isostatic adjustment, The Cryosphere, 7, 1499–1512.DOI：10.5194/tcd-6-3703-2012,2013.

Schumacher, M., King, M. A., Rougier. J., Sha. Z., Khan. S. A., Bamber, J. L. A new global gps data set for testing and improving modelled gia uplift rates. Geophysical Journal International, 214(3), 2164-2176.DOI:10.1093/gji/ggy235.2018.

An, M.,D. A. Wiens., Y. Zhao., M. Feng., A. A. Nyblade., M. Kanao., Y. Li., A. Maggi., J. J. Lévêque .: S-velocity model and inferred Moho topography beneath the Antarctic plate from Rayleigh waves, J. Geophys. Res. Solid Earth, 120(1), 359–383, doi:10.1002/2014JB011332,2005.

Rignot, E.; Bamber, J. L.; Van, d. B. M. R.; Davis, C.; Li, Y.; Van, d. B. W. J.; Van, M. E. Recent antarctic mass loss from radar interferometry and regional climate modeling. Nature Geoscience, 1(2), 106-110.DOI: 10.1038/ngeo102.2008.

Vander Wal, W., P. L. Whitehouse., E. J. O. Schrama.: Effect of GIA models with 3D composite mantle viscosity on GRACE mass balance estimates for Antarctica, Earth Planet. Sci. Lett., 414, 134–143.DOI：10.1016/j.epsl.2015.01.001

Ivins, E. R., and T. S. James.: Antarctic glacial isostatic adjustment: A new assessment, Antarct. Sci., 17(4), 541–553.DOI：10.1017/S0954102005002968 ,2005.

Heeszel, D. S., D. A. Wiens, S. Anandakrishnan., R. C. Aster., I. W. D. Dalziel., A. D. Huerta., A. A. Nyblade., T. J. Wilson., and J. P. Winberry.: Upper mantle structure of central and West Antarctica from array analysis of Rayleigh wave phase velocities, J. Geophys. Res. Solid Earth, 121, 1758–1775, doi:10.1002/2015JB012616,2016.

Zhang, B. , Wang, Z. , Li, F. , An, J. , Yang, Y. , Liu, J. . (2017). Estimation of present-day glacial isostatic adjustment, ice mass change and elastic vertical crustal deformation over the antarctic ice sheet. Journal of Glaciology, 63(240), 703-715. DOI:10.1017/jog.2017.37.2017.

Wolstencroft,M.,King,M.A. , Whitehouse,P.L. , Bentley,M.J . , Nield,G.A. , King,E.C ., McMillan, ., Shepherd, A. , Barletta, V. , Bordoni, A. , Riva, R.E.M., Didova, O., Gunter, B.C.: Uplift rates from a new high-density GPS network in Palmer Land indicate significant late Holocene ice loss in the southwestern Weddell Sea, Geophys. J. Int., 203(1), 737–754, doi:10.1093/gji/ggv327,2015.

Boening, C., M. Lebsock, F. Landerer, and G. Stephens.: Snowfall-driven mass change on the East Antarctic ice sheet, Geophys. Res. Lett., 39(21), 1–5, doi:10.1029/2012GL053316,2012.

Caption of Figures

Figure 1. The distribution of Global Positioning System (GPS) stations in Antarctica

Figure 2. The PA test results of ICs

Figure 3. The results of IC1-IC8 components (the black arrows are a positive spatial response, the red are a negative spatial response)

Figure 4. the residual time series (left) and raw time series (right) of GMEZ before and after regional filter using the ICA (blue lines are the raw time series and the orange are filtered time series).

Figure 5. The RMS values of the residual time series before and after applying the ICA filters (%)

Figure 6. Contributions of IC2, IC4,IC7,IC8 (gray lines) to CME and residual time series of atmosphere (red lines), non-tide(green lines) and continental water storage(blue lines) at site CAS1.

Figure 7. The GPS velocity field after applying noise analysis and AIC filter

Figure 8. Elastic velocity of GPS in Antarctic (mm yr^{-1})

Figure 9. The divided 6 subregionals in Antarctic. Red represent those within the North Antarctic Peninsula; yellow those within the South Antarctic Peninsula; balck those within the Amundsen Sea Embaymen; blue those within the Filchner-Ronne Ice Shelf; light green those within the Ross Ice Shelf; and brown those along coastal East Antarctica.

Figure 10. The uplift velocities of GIA models（mm yr^{-1}）

Figure 11. The summary statistics WM and WRMS, Median values are indicated in brackets (mm yr^{-1})

Figure 12. The discrepancies between the modeled and the observed GIA uplift rates estimated from different solutions computed at each GPS site (Red circles indicate places where the estimated GIA rates underestimate the observed velocities from GPS; blue circles indicate the converse.)

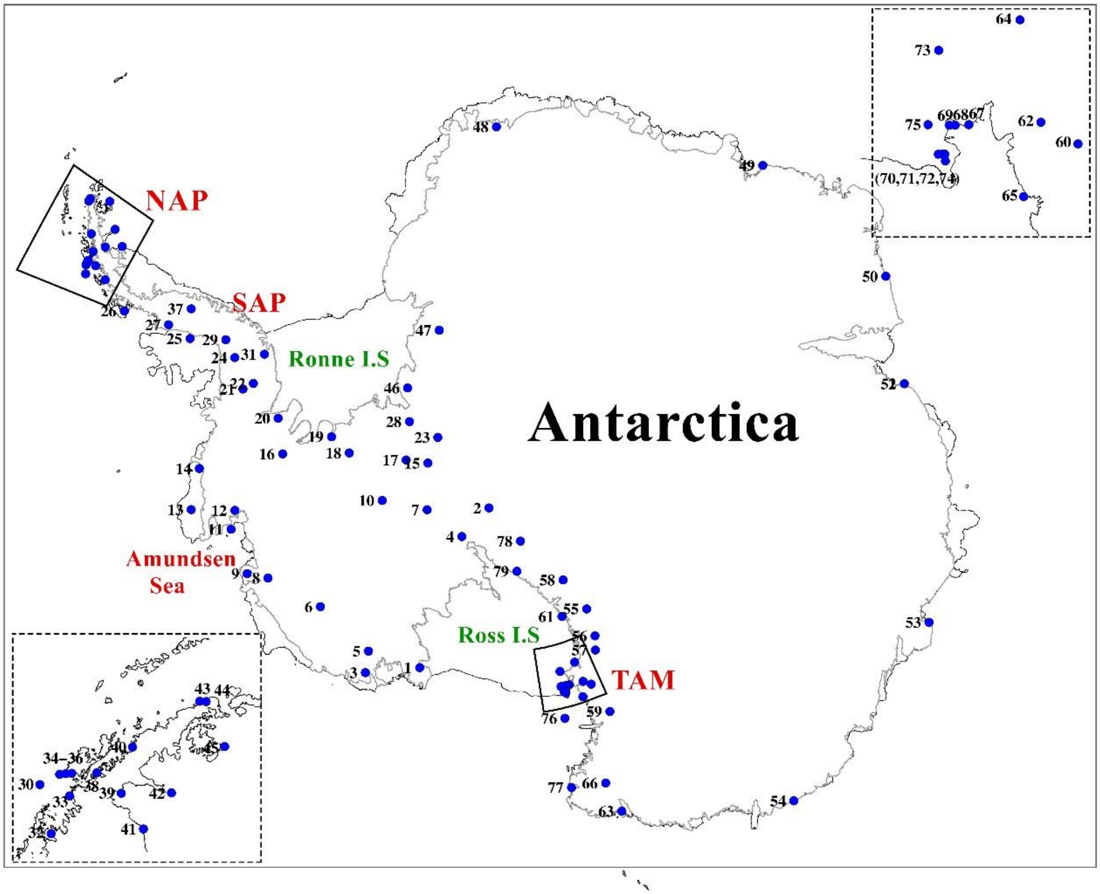

Figure 1. The distribution of Global Positioning System (GPS) stations in Antarctica

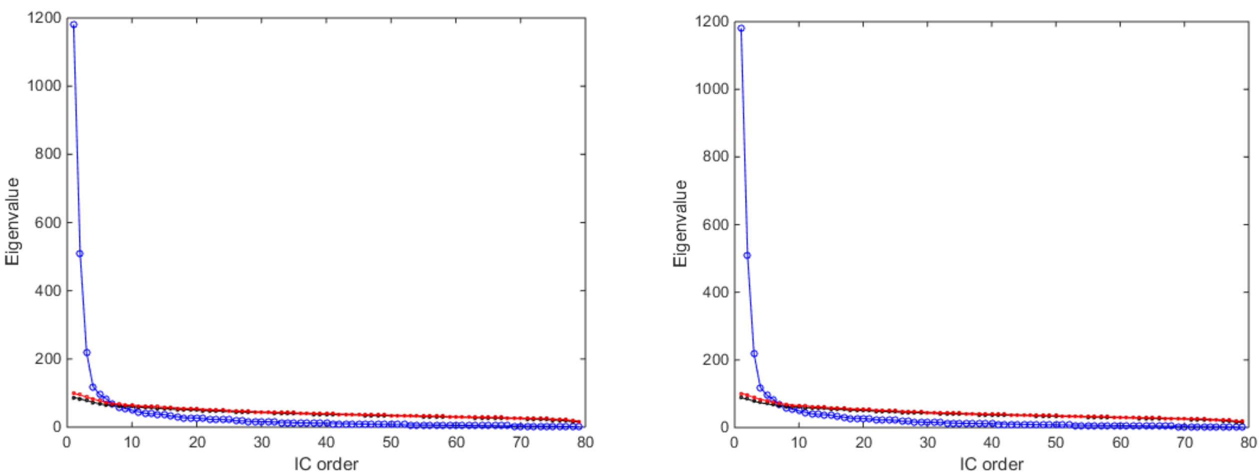

Figure 2. The PA test results of ICs (left is the results that without colored noise and right figure is the results using colored noise. Blue Line is the GPS data, black and red lines are the maximum and minimum values of simulation results)

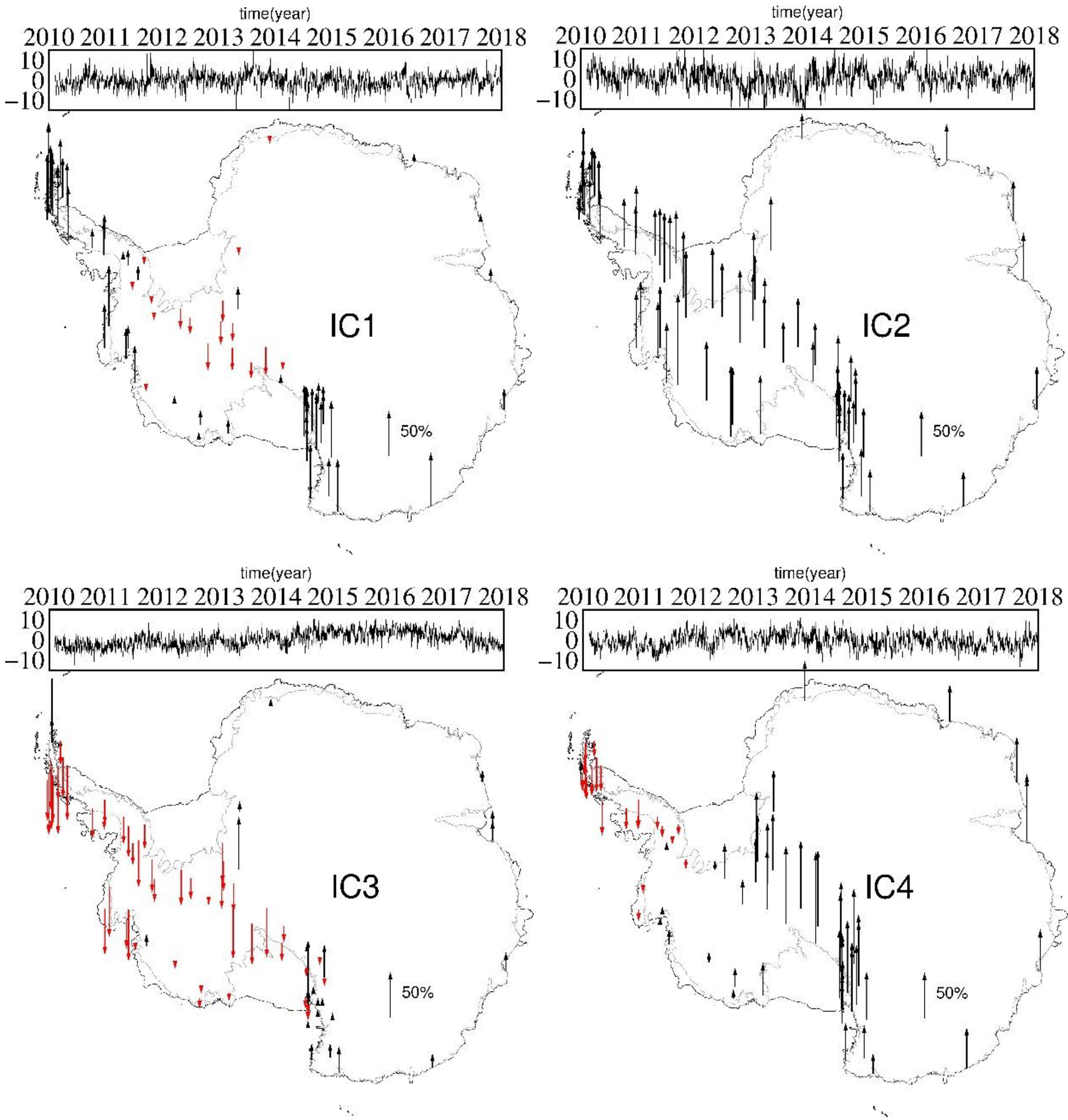

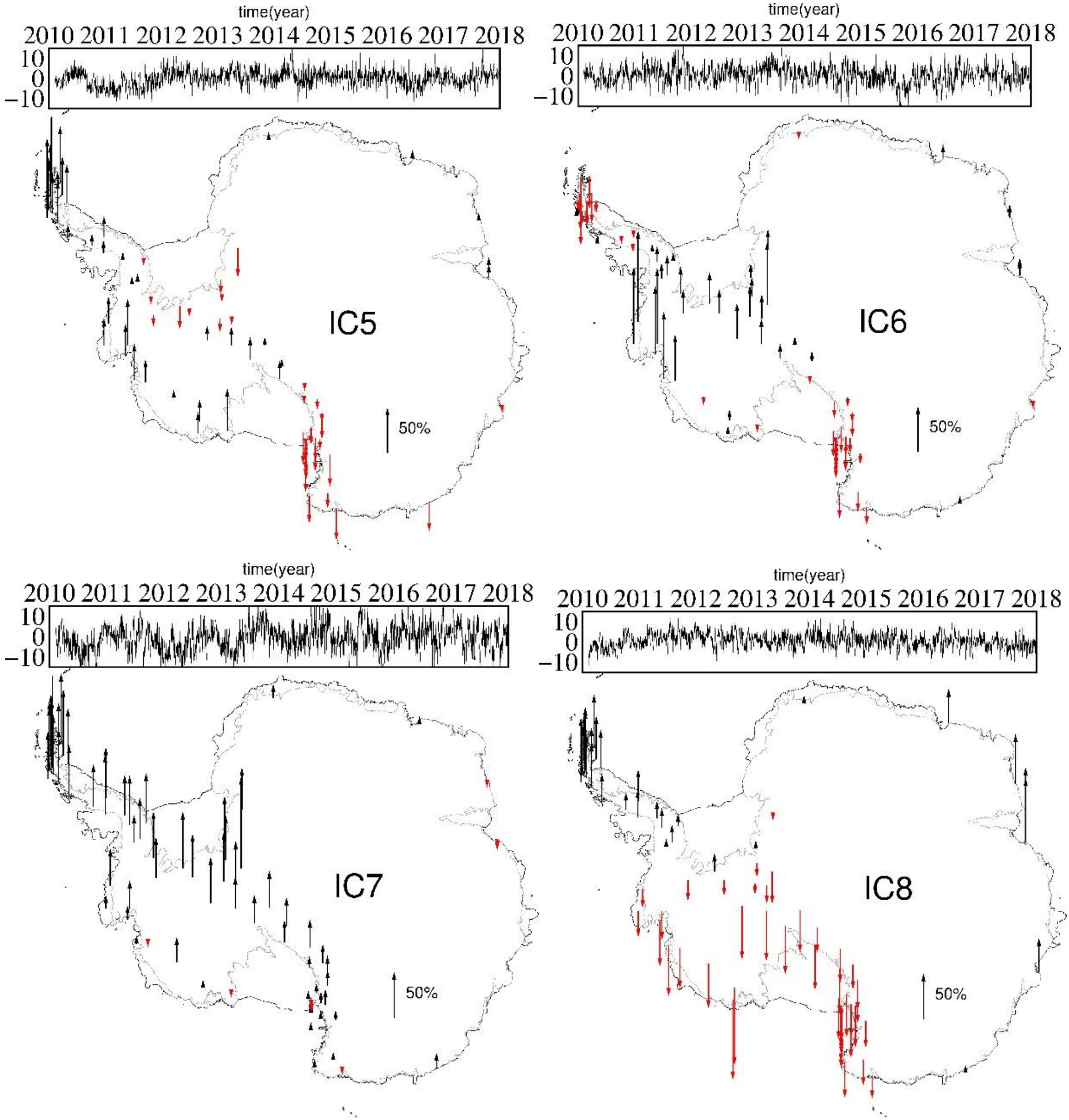

Figure 3. The results of IC1-IC8 components (the black arrows are a positive spatial response, the red are a negative spatial response)

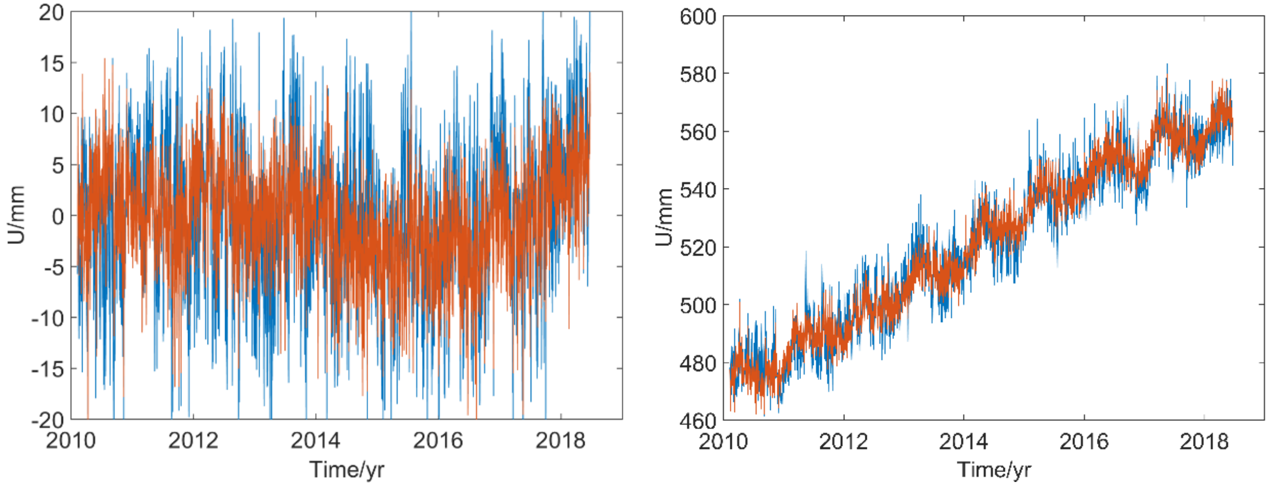

Figure 4. the residual time series (left) and raw time series (right) of GMEZ before and after regional filter using the ICA (blue lines are the raw time series and the orange are filtered time series).

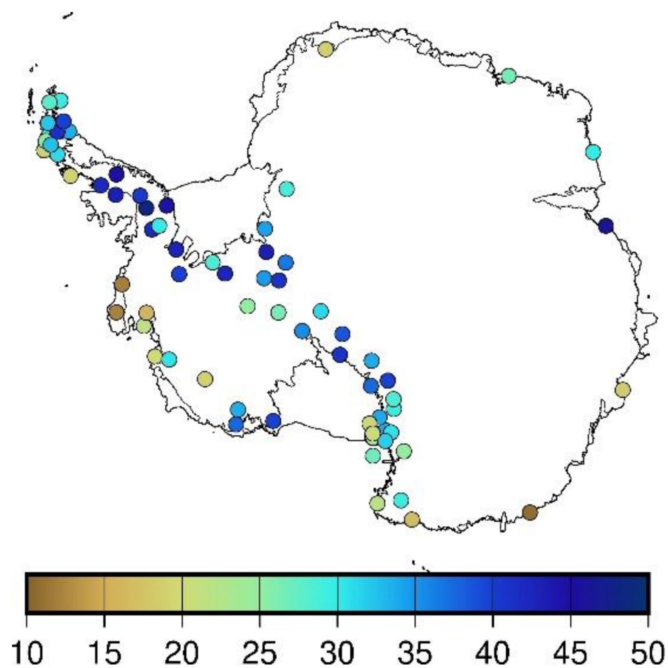

Figure 5. The RMS values of the residual time series before and after applying the ICA filters (%)

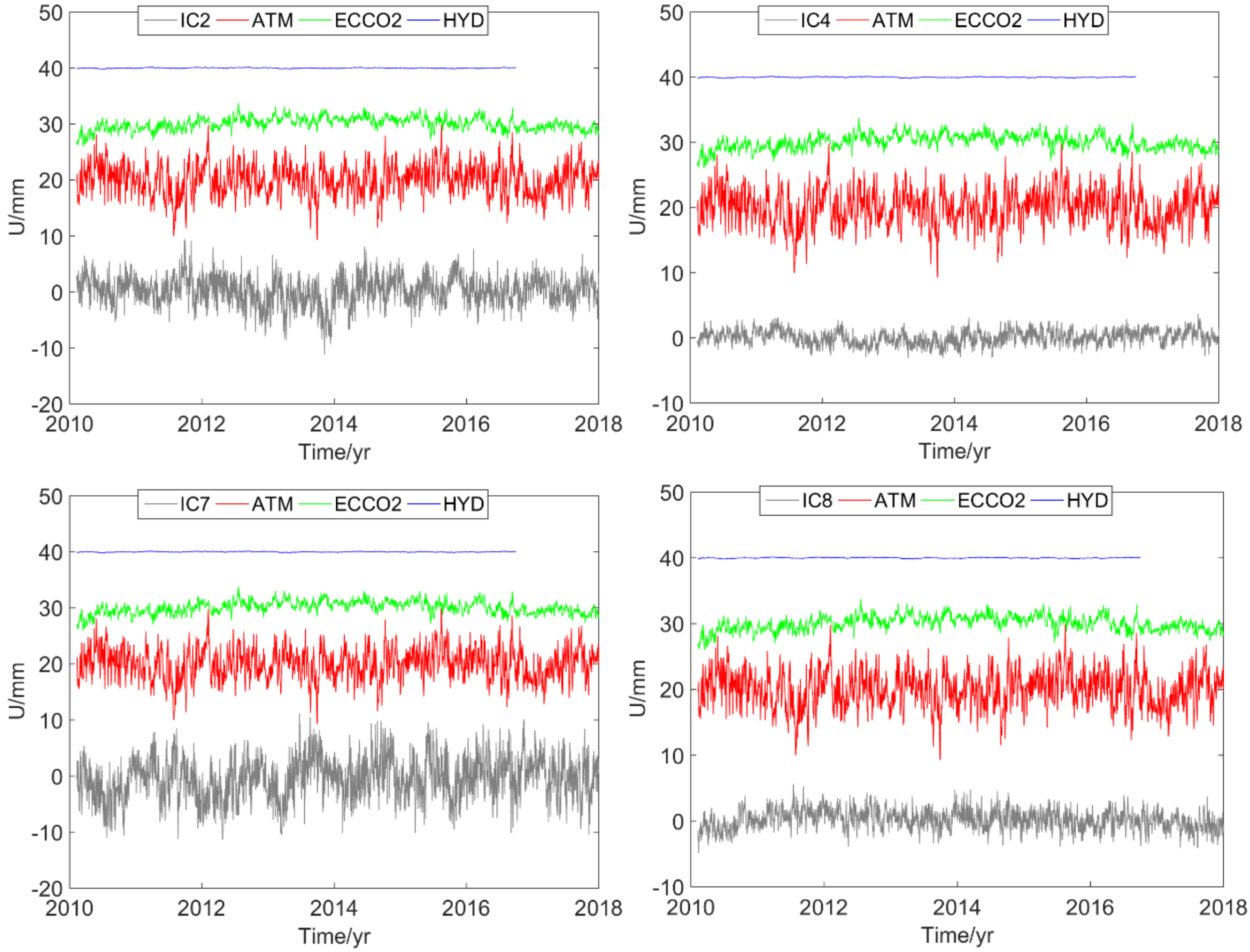

Figure 6. Contributions of IC2, IC4, IC7 and IC8 (gray lines) to CME and residual time series of atmosphere (red lines), non-tide(green lines) and continental water storage(blue lines) at site CAS1.

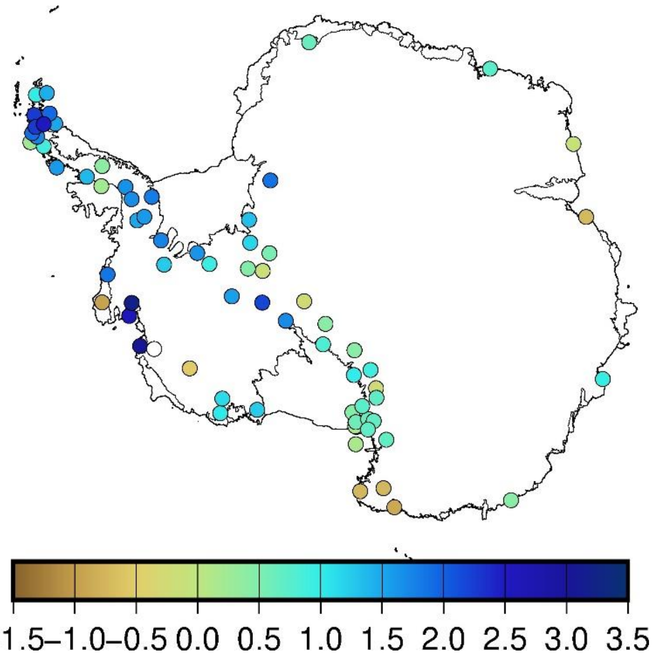

Figure 7. The GPS velocity field after applying noise analysis and AIC filter (mm yr^{-1})

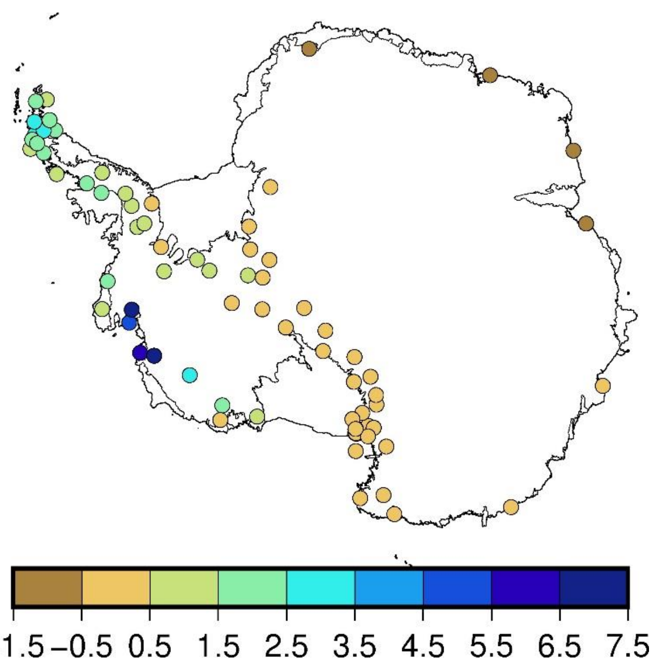

Figure 8. Elastic velocity of GPS in Antarctic (mm yr^{-1})

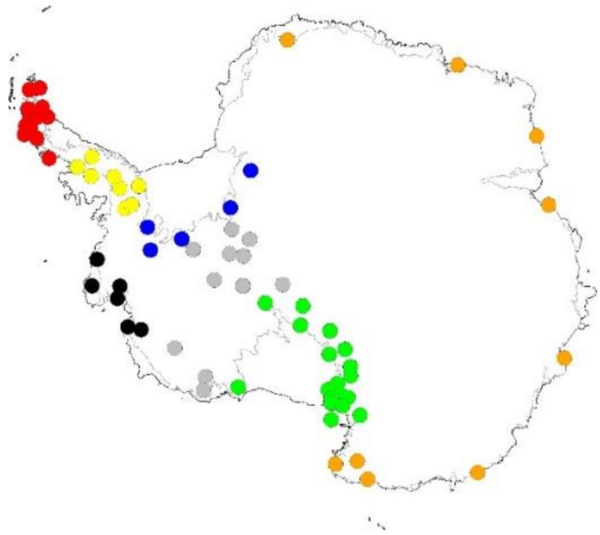

Figure 9. The divided 6 subregionals in Antarctic. Red represent those within the North Antarctic Peninsula; yellow those within the South Antarctic Peninsula; balck those within the Amundsen Sea Embaymen; blue those within the Filchner-Ronne Ice Shelf; light green those within the Ross Ice Shelf; and brown those along coastal East Antarctica.

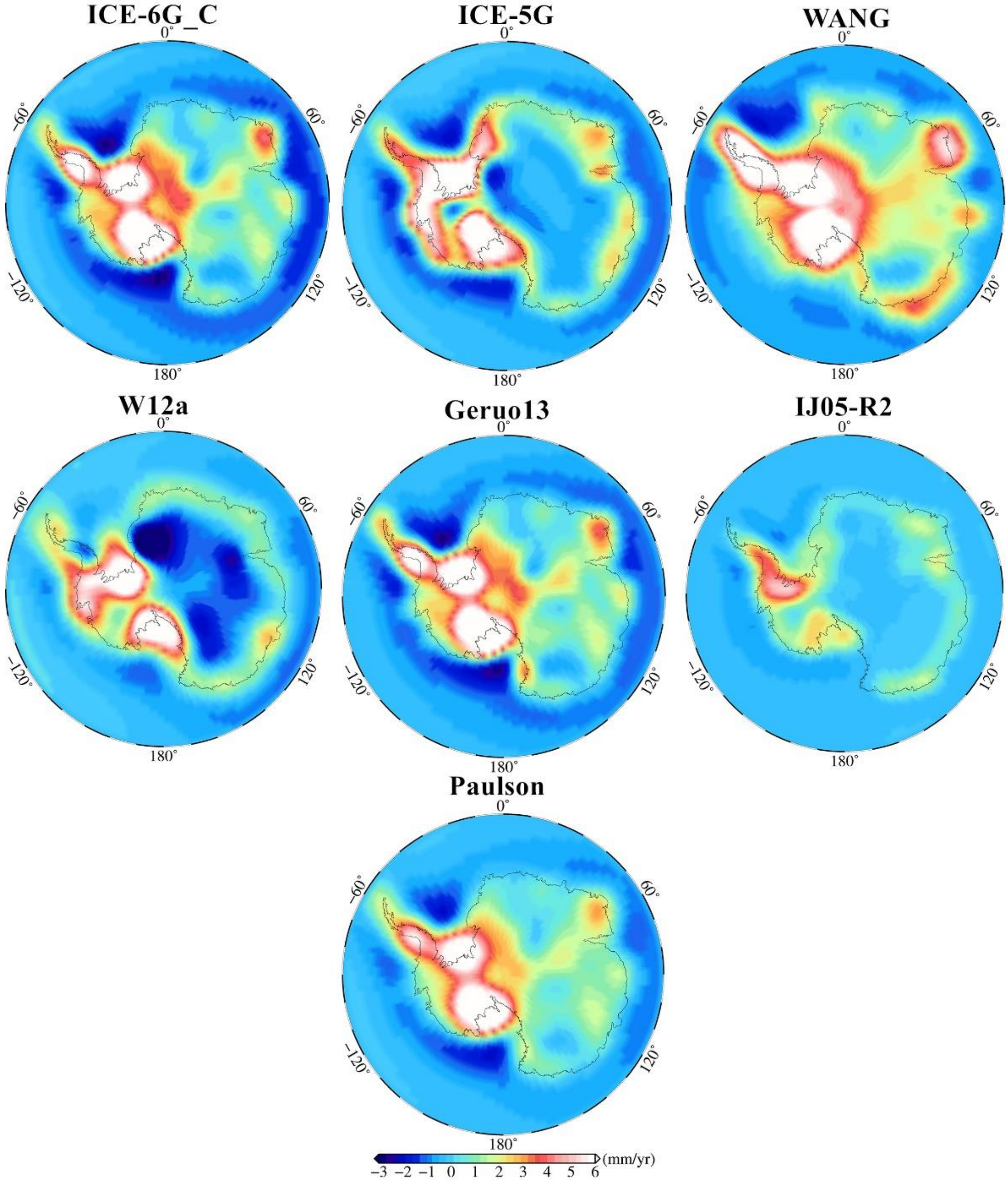

Figure 10. The uplift velocities of GIA models（mm yr^{-1}）

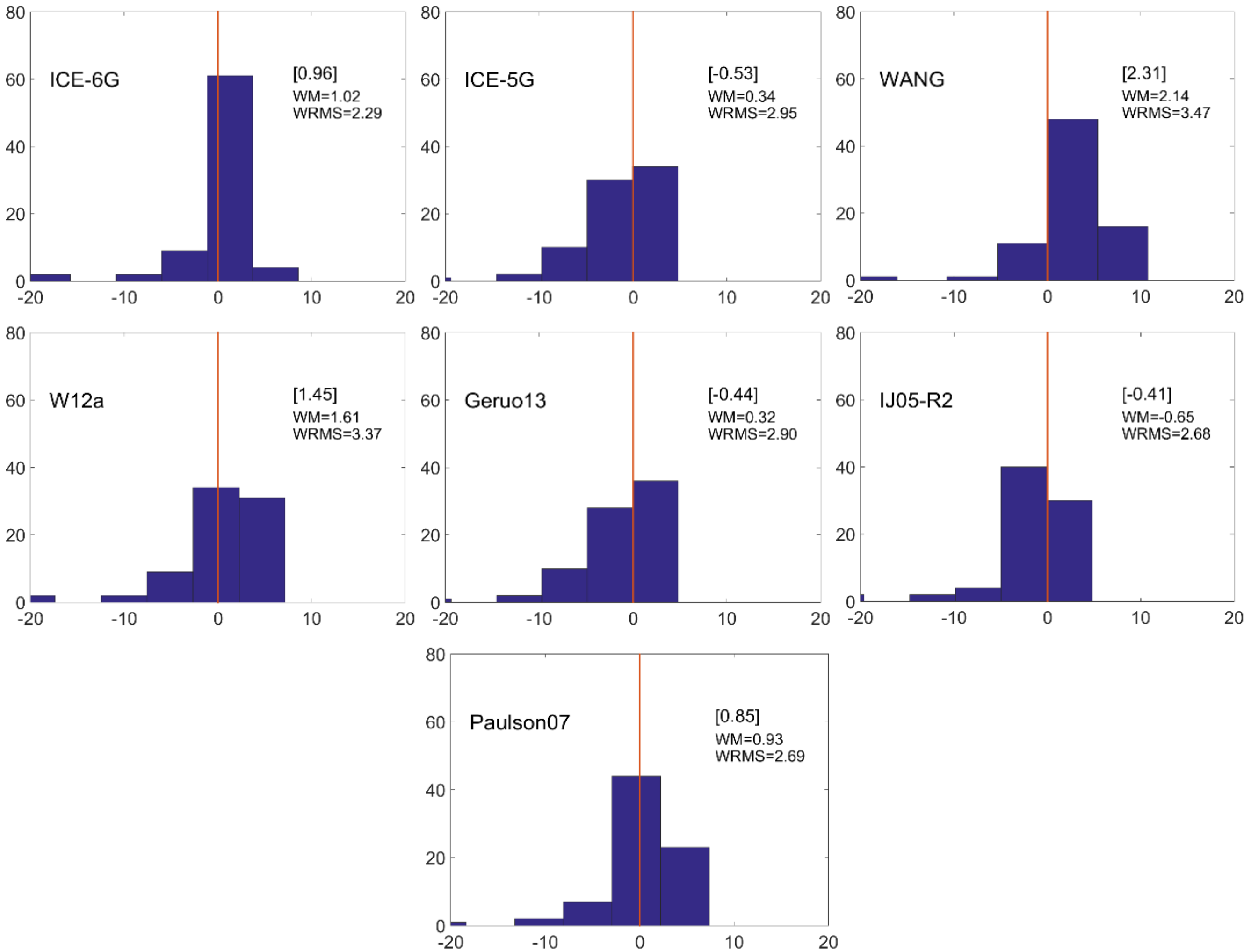

Figure 11. The summary statistics WM and WRMS, Median values are indicated in brackets (mm yr^{-1})

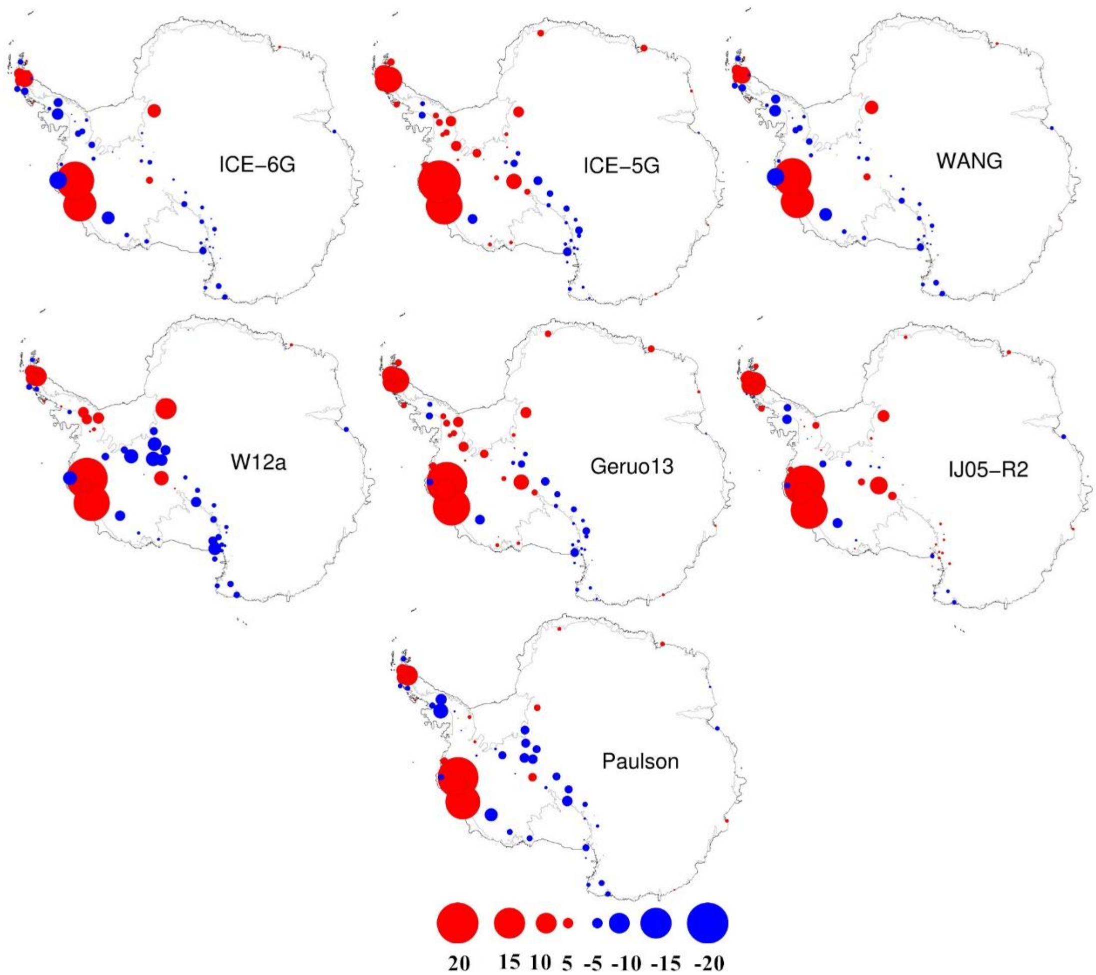

Figure 11. The discrepancies between the modeled and the observed GIA uplift rates estimated from different solutions computed at each GPS site (Red circles indicate places where the estimated GIA rates underestimate the observed velocities from GPS; blue circles indicate the converse.)

5 Tables

Table 1. The ONMs and corresponding velocities of GPS stations (mm yr^{-1})

Sites	Noise Model	Velocity	Sites	Noise Model	Velocity
ABBZ	WN+PL	-0.1±0.4	MCM4	WN+PL	-0.4±0.2
BACK	WN+FN	15.8±0.9	MCMD	WN+PL	0.1±0.2
BENN	WN+PL	9.9±0.2	MIN0	WN+PL	0.6±0.1

BERP	WN+PL	27.3±0.7	MKIB	WN+FN	6.2±0.5
BRIP	WN+PL	1.1±0.2	OHI2	WN+PL	1.1±0.5
BUMS	WN+FN	0.6±0.5	OHI3	WN+PL	1.9±0.6
BURI	WN+PL	1.2±0.1	PAL2	WN+PL	6.2±0.3
CAPF	WN+PL	4.1±0.3	PALM	WN+PL	6.2±0.3
CAS1	WN+PL	1.9±0.4	PALV	WN+PL	6.9±0.3
CLRK	WN+PL	2.5±0.1	PATN	WN+PL	2.9±0.3
COTE	WN+PL	1.0±0.1	PECE	WN+FN	0.8±0.5
CRAR	WN+PL	1.0±0.2	PHIG	WN+RW+GGM	-2.4±1.6
CRDI	WN+PL	3.3±0.1	PIRT	WN+PL	1.8±0.18
DAV1	WN+PL	-1.2±0.1	PRPT	WN+PL	1.6±0.8
DAVE	WN+PL	-2.4±0.2	RAMG	WN+FN	1.4±0.2
DEVI	WN+PL	2.0±0.1	RMBO	WN+PL	2.6±0.2
DUM1	WN+FN	0.6±0.8	ROB4	WN+PL	1.1±0.2
DUPT	WN+RW+GGM	10.9±1.3	ROBN	WN+PL	7.2±0.4
FALL	WN+PL	5.4±0.2	ROTH	WN+PL	4.7±0.7
FIE0	WN+PL	0.2±0.5	SCTB	WN+PL	-0.3±0.14
FLM5	WN+PL	1.1±0.1	SDLY	WN+PL	-0.8±0.2
FONP	WN+PL	15.0±0.4	SPGT	WN+PL	10.9±0.6
FOS1	WN+PL	0.3±0.4	STEW	WN+FN	0.7±0.6
FTP4	WN+PL	1.3±0.1	SUGG	WN+FN	4.7±0.5
GMEZ	WN+PL	5.4±0.3	SYOG	WN+PL	1.3±0.4
HAAG	WN+PL	5.8±0.3	THU4	WN+PL	-1.8±0.6
HOOZ	WN+PL	-0.3±0.5	TOMO	WN+FN	52.6±1.0
HOWE	WN+FN	-0.3±0.4	TRVE	WN+PL	3.5±0.3
HOWN	WN+PL	2.9±0.2	VESL	WN+PL	1.0±0.7
HUGO	WN+FN	0.3±0.8	VL01	WN+PL	-1.2±1.1
IGGY	WN+FN	0.6±0.3	VL12	WN+PL	-1.3±0.7
INMN	WN+FN	32.6±1.1	VL30	WN+FN	-1.6±1.8
JNSN	WN+PL	5.0±0.4	VNAD	WN+PL	5.6±0.4

LNTK	WN+FN	4.2±0.8	WHN0	WN+PL	0.3±0.2
LPLY	WN+FN	6.6±1.2	WHTM	WN+RW+GGM	4.5±1.5
LWN0	WN+PL	1.7±0.7	WILN	WN+PL	4.9±0.4
MACG	WN+FN	0.2±0.5	WLCH	WN+PL	0.5±0.4
MAW1	WN+PL	-0.1±0.1	WLCT	WN+FN	-0.2±0.6
MBIO	WN+PL	3.8±0.5	WWAY	WN+RW+GGM	6.8±2.8
MCAR	WN+PL	2.1±0.2			

Table 2. The maximum, minimum, mean values and standard deviation of 7 GIA models uplift velocties（>60 °S）

GIA	Max(mm yr^{-1})	Min(mm yr^{-1})	Mean(mm yr^{-1})	Std(mm yr^{-1})
ICE6G_C	13.50	-2.20	0.71	1.15
ICE5G	13.90	-2.80	1.58	1.10
WANG	15.27	-2.13	2.60	1.15
W12a	10.33	-6.11	0.58	0.97
Geruo13	15.00	-2.70	1.34	1.19
IJ05-R2	5.24	-0.88	0.22	0.45
Paulson	12.46	-1.98	1.50	1.07

Table 3. The WM results in North Antarctic Peninsula (NAP), South Antarctic Peninsula (SAP), Amundsen Sea Embayment (ASE), Margins of the Ross (ROSS), Filscher-Ronne Ice Shelves(FRIS), and East Antarctica (EA)a

Model	NAP(15)		SAP(8)		ASE(5)		ROSS(25)		FRIS(5)		EA(8)		Antarctica(79)	
	WM	WM*	WM	WM*	WM	WM*	WM	WM*	WM	WM*	WM	WM*	WM	WM*
ICE6G_C	-1.18	-1.49	2.57	2.42	-4.68	-3.78	1.25	1.16	1.92	1.38	-0.09	0.49	0.48	1.02
ICE5G	-4.80	-5.21	-1.71	-1.14	-9.98	-9.04	1.35	1.58	-2.72	-0.34	-1.03	-0.57	-1.04	0.34
WANG	2.28	1.98	4.22	5.29	-8.72	-7.81	1.89	1.46	2.62	2.46	1.76	2.47	1.78	2.14
W12a	-1.91	-2.27	-1.98	-2.22	-6.27	-5.42	2.37	2.06	2.75	2.11	0.39	0.93	0.80	1.61
Geruo13	-4.51	-4.91	-1.64	-1.07	-9.89	-8.95	1.33	1.52	-2.65	-0.32	-1.12	-0.63	-1.01	0.32
IJ05R2	-3.71	-4.06	0.25	0.59	-10.02	-9.14	-0.86	-0.91	0.51	0.73	-0.16	0.65	-1.38	-0.65
Paulson	-2.04	-2.40	1.65	2.33	-10.06	-9.16	1.07	0.72	1.45	1.70	0.05	1.01	0.10	0.93

[a] The number of sites in each area is indicated in parentheses; * represents the results of applying ICA filtering and AIC noise analysis.

Table 4. The WRMS results in North Antarctic Peninsula (NAP), South Antarctic Peninsula (SAP), Amundsen Sea Embayment (ASE), Margins of the Ross and Filscher-Ronne (FRIS) Ice Shelves, and East Antarctica (EA)[a]

Model	NAP(15)		SAP(8)		ASE(5)		ROSS(25)		FRIS(5)		EA(8)		Antarctica(79)	
	WRMS	WRMS*	WRMS	WRMS*	WRMS	WRMS*	WRMS	WRMS*	WRMS	WRMS*	WRMS	WRMS*	WRMS	WRMS*
ICE6G_C	3.02	3.31	2.89	2.96	11.20	11.83	1.47	1.35	2.37	2.22	0.87	1.10	3.49	2.29
ICE5G	5.72	6.14	2.86	2.97	14.02	14.22	1.98	1.92	3.16	2.52	1.37	1.29	4.61	2.95
WANG	3.62	3.57	5.32	6.35	13.28	13.55	2.55	1.93	4.09	3.99	2.94	3.14	4.70	3.47
W12a	3.53	3.88	2.85	3.46	11.90	12.37	2.91	2.67	3.59	3.01	0.99	1.49	4.27	3.37
Geruo13	5.47	5.88	2.81	2.93	13.96	14.16	1.93	1.85	3.09	2.50	1.45	1.32	4.54	2.9
IJ05R2	4.76	5.14	1.80	2.35	14.13	14.26	1.32	1.22	2.15	2.32	1.10	1.45	4.24	2.68
Paulson	3.58	3.96	2.88	3.61	14.14	14.30	1.64	1.16	2.58	2.83	1.40	1.54	4.22	2.69

[a] The number of sites in each area is indicated in parentheses; * represents the results of applying ICA filtering and AIC noise analysis.